Dissertation

Investigation of the intestinal ultrastructure, apoptosis and status of the tight junctions in the early phase of murine sepsis.

submitted by

Mag. rer. nat. Beate Obermüller

for the Academic Degree of

Doctor of Medical Science (Dr. scient. med.)

at the

Medical University of Graz

Department of Pediatric and Adolescent Surgery

under the Supervision of

Assoc. Prof. Priv.-Doz. Dr. med. univ. Christoph Castellani

2020

Ehrenwörtliche Erklärung

Ich erkläre ehrenwörtlich, dass ich die vorliegende Arbeit selbständig und ohne fremde Hilfe verfasst, andere als die angegebenen Quellen nicht benutzt und die den Quellen wörtlich oder inhaltlich entnommenen Stellen als solche kenntlich gemacht habe. Diese Arbeit wurde bisher in gleicher oder ähnlicher Form keiner anderen Prüfungsbehörde vorgelegt und auch nicht veröffentlicht. Die vorliegende Fassung entspricht der eingereichten elektronischen Version.

Affidavit

I hereby declare that this thesis is my own original work and that I have fully acknowledged by name all of those individuals and organizations that have contributed to the research for this thesis. Due acknowledgment has been made in the text to all other material used. Throughout this thesis and in all related publications I followed the "Standards of Good Scientific Practice and Ombuds Committee at the Medical University of Graz."

This thesis reproduces parts of the following publication authored by the doctoral candidate:

Obermüller B, Frisina N, Meischel M, Singer G, Stanzl-Tschegg S, Lichtenegger H, Kolb D, Klymiuk I, Till H, Castellani C. Examination of intestinal ultrastructure, bowel wall apoptosis and tight junctions in the early phase of sepsis. Sci Rep. 2020 Jul 13; 10(1):11507. doi: 10.1038/s41598-020-68109-9. PMID: 32661347 PMCID: PMC7359326

The following co-authors actively contributed to this dissertation and authorize the use of their personal data:

- Noemi Frisina MSc., Institute of Physics and Materials Science, University of Natural Resources and Life Sciences, Vienna, Austria
- DI Dr. Martin Meischel, Institute of Physics and Materials Science, University of Natural Resources and Life Sciences, Vienna, Austria
- Assoz. Prof. Priv.-Doz. Dr. med. univ. Georg Singer, Department of Paediatric and Adolescent Surgery, Medical University of Graz, Graz, Austria
- Univ.-Prof.in i.R. Dr.in phil. Stefanie Stanzl-Tschegg, Institute of Physics and Materials Science, University of Natural Resources and Life Sciences, Vienna, Austria
- Univ. Prof.in Mag.a Dr.in rer. nat. Helga Lichtenegger, Institute of Physics and Materials Science, University of Natural Resources and Life Sciences, Vienna, Austria
- Priv.-Doz. Mag.a Dr.in rer. nat. Dagmar Kolb, Core Facility Ultrastructure Analysis, Center for Medical Research, Division of Cell Biology, Histology and Embryology, Gottfried Schatz Research Center, Medical University of Graz, Graz, Austria

- Mag.[a] Dr.[in] rer. nat. Ingeborg Klymiuk, Core Facility Molecular Biology, Center for Medical Research, Medical University of Graz, Graz, Austria
- Univ. Prof. Dr. med. Dr. med. habil. Holger Till, Department of Paediatric and Adolescent Surgery, Medical University of Graz, Graz, Austria
- Assoz. Prof. Priv.-Doz. Dr. med. univ. Christoph Castellani, Department of Paediatric and Adolescent Surgery, Medical University of Graz, Graz, Austria

Mag. Beate Obermüller

Graz, September 2020

Acknowledgements

The present work has been conducted in association with the Doctoral School “Molecular Medicine and Inflammation” at the Medical University of Graz, Austria.

The project was funded by the Preidler Szolar grant of the MeFo Graz (to Christoph Castellani) and the inVITA Gesellschaft zur Förderung der Gesundheit unserer Kinder (to Georg Singer). Doctoral student Beate Obermüller received funding from the Medical University of Graz through the Doctoral School Molecular Medicine and Inflammation (MMI).

„Wirkliches Neuland in einer Wissenschaft kann wohl nur gewonnen werden, wenn man an einer entscheidenden Stelle bereit ist, den Grund zu verlassen, auf dem die bisherige Wissenschaft ruht, und gewissermaßen ins Leere zu springen.“

Werner Heisenberg, dt. Physiker, Nobelpreis 1932

Danksagung

Mein besonderer Dank gilt meinen Doktorvätern Assoz. Prof. Priv.-Doz. Dr. med. univ. Christoph Castellani und Assoz. Prof. Priv.-Doz. Dr. med. univ. Georg Singer, die mich in allen Phasen dieser Arbeit gefördert und unterstützt haben und stets eine Diskussion auf Augenhöhe zuließen.

Herzlichen Dank den Kooperationspartnern Univ. Prof.in Mag.a Dr.in rer. nat. Helga Lichtenegger, Univ.-Prof.in i.R. Dr.in phil. Stefanie Stanzl-Tschegg, DI Dr. Martin Meischel und Noemi Frisina MSc. der Universität für Bodenkultur in Wien für die enge Zusammenarbeit in ihrem Experten-Bereich.

Des Weiteren möchte ich mich bei Anna Kuesz bedanken, die meine Arbeit durch ihre Kenntnisse und Bereitschaft, Neues zu probieren, sehr bereichert hat.

Für die finanzielle Unterstützung möchte ich mich bei der MeFo Graz mit dem Preidler Szolar Stipendium (an Christoph Castellani), der inVITA Gesellschaft zur Förderung der Gesundheit unserer Kinder (an Georg Singer) und der Doc-School Molecular Medicine and Inflammation (MMI) der Medizinischen Universität Graz bedanken.

Dr.in Birgit Reininger-Gutmann danke ich für die Möglichkeit, diese Arbeit trotz anderer Aufgabenstellung und anderem Wirkungskreis einreichen zu dürfen.

Bei meiner Familie, die immer an mich geglaubt hat und nie aufgehört hat, mich in allen Belangen zu unterstützen.

Ganz besonderer Dank gilt meinem Mann Dietmar, der meine Ideen und Sonderwünsche gelassen akzeptiert und mir stets Platz lässt, meine Träume zu verwirklichen.

LIST OF ABBREVIATIONS

AJ	Adherens Junction
BAD	BCL2 Associated Agonist of Cell Death
BAK	BCL2 Homologous Antagonist
BAX	Apoptosis Regulator, BCL2 Like Protein 4
BCL2	B-Cell Lymphoma 2; Regulator Protein for Apoptosis
CRP	C Reactive Protein
CLDN	Claudin
CLP	Cecal Ligation and Puncture
ELISA	Enzyme Linked immunosorbent Assay
ELMI	Electron Microscopy
FiO2	Inspiratory Fraction of Oxygen
FITC	Fluorescence Isothiocyanat Dextran
GCS	Glasgow Coma Score
H&E	Hematoxylin and Eosin
ICU	Intensive Care Unit
I-FABP	Intestinal Free Fatty Acid Binding Protein
IEC	Intestinal Epithelial Cell
IL	Interleukin
INF- γ	Interferon gamma
IQR	Interquartile Range
kD	Kilodalton
LPS	Lipopolysaccharide
MAP	Mean Arterial Pressure
Min	Minute

MLCK	Myosin Light Chain Kinase
MUC	Mucin
NFkB	Nucleus Factor Kappa B
OCLN	Occludin
PaO2	Arterial Partial Pressure of Oxygen
PAMP	Pathogen Associated Molecular Pattern
PCR	Polymerase Chain Reaction
PCT	Procalcitonin
SP-A	Surfactant Protein A
SP-D	Surfactant Protein D
SMAD	Homology to the *Caenorhabditis elegans* SMA ("small" worm phenotype") and Drosophila MAD ("Mothers Against Decapentaplegic") family of genes
SNAIL	Zinc Finger Protein
SOFA-Score	Sequential Organ Failure Assessment Score
TEM	Transmission Electron Microscopy
TGF-β	Transforming Growth Factor Beta
TJ	Tight Junction
TJP-1	Tight Junction Protein 1
TLR	Toll Like Receptor
TNF-α	Tumor Necrosis Factor Alpha
US	United States

ABSTRACT

Introduction: Sepsis is a life-threatening organ dysfunction caused by a dysregulated host response to infection. It is responsible for a large proportion of deaths on non-cardiologic intensive care units and is thus referred to as “silent killer”. Among many other organs, sepsis may cause alterations of the gut barrier, one of the most important barriers of the human body, leading to increased bowel wall permeability. This hyper-permeability can be caused by either apoptosis of the intestinal epithelium or altered status, permeability or porosity of tight junctions. It leads to passage of bacteria or bacterial toxins to the body, further fueling the inflammatory process and aggravating the patients´ conditions. This project aims to elucidate the underlying mechanisms for intestinal hyper-permeability in the early phase of sepsis.

Methods: Eighteen male C57Bl/6 wild type mice were split to two groups. All mice received one single gavage of fluorescein isothiocyanate-dextran (FITC) 30min before intervention. One group (n=10) underwent cecal ligation and puncture (CLP) to induce sepsis. The other group (n=8) was sham operated. Animals were euthanized 8 hours after the induction of sepsis. A clinical sepsis score was applied to all mice. Serum FITC Dextran levels were determined by photometry. Serum pro-inflammatory cytokines were examined by Luminex® ELISA. Bowel wall inflammation was examined histologically. Electron microscopy was performed to assess the surface of ileum and colon (scanning electron microscopy, SEM) and the intercellular junctional complex (transmission electron microscopy, TEM). Additional information of tight junctions (TJ) was gained by PCR and ELISA for TJ components (claudin 2, claudin 4, occludin and tight junction protein 1). Intestinal epithelial cell (IEC) apoptosis was addressed by HOECHST staining and apoptosis marker PCR (Bax, Bak, Bad, Caspase-3, Lamin-B,

Bcl-2) in ileum samples. The cellular ultrastructure was examined with Small Angle X-Ray Scattering (SAXS).

Results: Septic animals exhibited significantly increased permeability for FITC 8h post-operatively. The clinical sepsis score and significantly increased serum interleukin-6, tumor-necrosis-factor-alpha and interleukin-1-beta confirmed sepsis. Septic animals showed significant bowel wall inflammation of ileum and colon samples. PCR revealed significantly increased expression of claudin 2 and decreased expressions of claudin 4, tight junction protein 1 and occludin as signs for increased TJ porosity. Light microscopy showed significant dilatation of intercellular spaces at the basal sections of IECs in septic animals confirmed by increased intercellular spaces at the level of TJs and adherens junctions in electron microscopy (TEM). HOECHST staining and PCR of ileum samples for apoptosis markers proved no differences in intestinal epithelial cell apoptosis between the groups. The bowel surface showed no significant differences between the groups in SEM surface analysis or conventional histology. In small angle X-ray scattering no increase in number or size of nano-pores could be shown in the bowel wall.

Conclusions: Intestinal hyper-permeability in septic animals is most likely caused by alterations of intercellular contacts and TJ porosity and not by apoptosis or altered ultrastructure of intestinal epithelial cells in this murine model of early sepsis.

ZUSAMMENFASSUNG

Einleitung: Sepsis wird als lebensbedrohliche Entzündung durch eine Regulationsstörung der Immunantwort definiert. Sie ist für einen großen Anteil der Todesfälle auf nicht kardiologischen Intensivstationen verantwortlich und stellt somit ein erhebliches gesundheitliches Problem dar. Neben einer Vielzahl von Organfehlfunktionen bis hin zum Multiorganversagen beeinflusst die Sepsis auch die Darmwandbarriere. Diese stellt eine der wichtigsten Barrieren des menschlichen Körpers dar. Eine gesteigerte Permeabilität, die durch erhöhte Spiegel pro-inflammatorische Zytokine im Rahmen der Sepsis ausgelöst wird, führt zur Leckage von Bakterien oder bakteriellen Toxinen in den Körper. Dadurch kommt es zu einer weiteren Verstärkung der Entzündungsreaktion und somit zur Verschlimmerung des klinischen Zustandes. Ziel dieser Studie war es, die der Hyperpermeabilität zugrundeliegenden Mechanismen in der Frühphase der Sepsis im Mausmodell zu untersuchen.

Methode: Achtzehn männliche C57Bl/6 Mäuse wurden in zwei Gruppen aufgeteilt. Allen Mäusen wurde 30 Minuten vor der Intervention Fluoreszenzisothiozyanat-Dextran (FITC) gavagiert. Bei einer Gruppe (n=10) wurde in Vollnarkose eine Ligatur und Punktion des Caecums durchgeführt. Die andere Gruppe (n=8) wurde ohne Punktion oder Ligatur sham operiert. Die Tiere wurden 8 Stunden post-operativ in Narkose euthanasiert. Bei allen Mäusen wurde ein klinischer Sepsis Score erhoben. Die Serum FITC Dextran Werte wurden fotometrisch bestimmt. Pro-inflammatorische Zytokine im Serum wurden mittels Luminex® ELISA bestimmt. Die Entzündung der Darmwand von Ileum und Colon wurde histologisch evaluiert. Mittels Elektronenmikroskopie wurde eine Oberflächenanalyse (scanning electron microscopy, SEM) von Ileum und Colon und eine Evaluierung der Tight Junctions (TJ)

(transmission electron microscopy, TEM) im Ileum durchgeführt. Die Untersuchung der TJ wurde durch Bestimmung von TJ Komponenten (Claudin 2, Claudin 4, Occludin und Tight Junction Protein 1) mittels PCR und ELISA erweitert. Mittels HOECHST Färbung und PCR von Apoptosemarkern (Bax, Bak, Bad, Caspase-3, Lamin-B, Bcl-2) von Ileumproben wurde die Apoptoserate der IEC bestimmt. Mittels Kleinwinkelröntgendiffraktion (Small Angle X-Ray Scattering, SAXS) wurde eine Analyse der zellulären Ultrastruktur durchgeführt.

Ergebnisse: Septische Tiere zeigten eine signifikante Hyperpermeabilität für FITC Dextran. Der septische Zustand wurde durch einen klinischen Sepsis-Score bewiesen und von erhöhten Serumwerten pro-inflammatorischer Zytokine (Interleukin 1 beta, Tumor Nekrose Faktor Alpha und Interleukin 6) untermauert. In der PCR zeigten sich ein Anstieg von Claudin-2 und ein Abfall von Claudin 4, Occludin und Tight Junction Protein 1 als Zeichen einer erhöhten Porosität der TJ. Die Lichtmikroskopie und die TEM ergaben erweiterte Interzellularräume auf Höhe der TJ und Adherens Junctions als Zeichen für eine Öffnung des junctionalen Komplexes. Weder HOECHST Färbung noch PCR ergaben Hinweise auf eine gesteigerte Apoptoserate im Rahmen der Sepsis. Die Analyse der Darmoberfläche in der Histologie und der SEM zeigte ebenfalls keine signifikanten Gruppenunterschiede. Mittels SAXS konnte kein signifikanter Unterschied in Hinblick auf eine veränderte zelluläre Ultrastruktur der Darmepithelzellen gewonnen werden.

Schlussfolgerungen: Die intestinale Hyperpermeabilität in diesem Frühmodell der Sepsis wurde durch eine Kombination von erhöhter Porosität der TJ und einer Störung des junctionalen Komplexes mit erweiterten TJ verursacht. Weder Apoptose noch Veränderungen der zellulären Ultrastruktur spielten in diesem Mausmodell der Frühphase der Sepsis eine Rolle.

Table of Contents

Introduction

Definition of Sepsis

Currently, sepsis is defined as “life threatening organ dysfunction caused by a dysregulated host response to infection” (1, 2). This infection may be triggered by bacteria, viruses, fungi or parasites with bacteria being the most frequent. Clinically, septic patients show alterations in a wide variety of different parameters such as hyper- or hypothermia, elevated heart rate, tachypnea, edema or fluid imbalance, hyperglycemia, altered mental status, leukocytosis or leucopenia, elevated plasma c-reactive protein (CRP) or procalcitonin (PCT), arterial hypotension, decreased oxygen saturation, increased cardiac index, acute oliguria, hyperbilirubinemia, coagulopathy, increased creatinine, ileus, thrombocytopenia, increased capillary refill time (impaired peripheral perfusion) and hyperlactatemia (3). Many of these factors are summed up in the sequential organ failure assessment score (SOFA-Score) (TABLE 1) (4).

A healthy patient without pre-existing organ pathology has a SOFA Score of 0. A SOFA-Score ≥2 with assumed/proven infection is associated with a mortality of ≥10% (2).

In the daily routine patients with sepsis can either improve under medical therapy or progress towards severe sepsis or septic shock. Severe sepsis is a frequent syndrome and associated with a high hospital mortality (5). It is defined as sepsis leading to sepsis-induced tissue hypo-perfusion or organ dysfunction (3). In severe cases hypotension persists despite fluid resuscitation causing a septic shock (3).

Table 1: SOFA-Score

	0	1	2	3	4
PaO_2/FiO_2	≥400mmHg	300-400mmHg	200-300mmHg	Invasive ventilation 100-200mmHg	Invasive ventilation <100mmHg
Platelet count	≥150x10^3/µl	100-150 x10^3/µl	50-100x10^3/µl	20-50x10^3/µl	<20x10^3/µl
Serum bilirubin	<1.2mg/dl	1.2-1.9mg/dl	2.0-5.9mg/dl	6.0-11.9mg/dl	>12.0mg/dl
Circulation	MAP >70mmHg	MAP <70mmHg	Dopamine <5[1] or Dobutamine (any dosage)	Dopamine 5.1-15[1] or Adrenaline/ Noradrenaline ≤0.1[1]	Dopamine >15[1] or Adrenaline/ Noradrenaline >0.1[1]
GCS	15	13-14	10-12	6-9	<6
Serum creatinine	<1.2mg/dl	1.2-1.9mg/dl	2.0-3.4mg/dl	3.5-4.9mg/dl	>5.0mg/dl

Epidemiology of Sepsis

Sepsis is also referred to as “silent killer” on intensive care units (ICUs) and ranks among the leading causes of death in western countries (6). Martin and Sovillo have reported 1,017,616 deaths in the United States (US) due to sepsis in a six-year period (6% of all deaths in this period) (7). Focusing on ICUs, an observational cohort study revealed severe sepsis as leading cause of death in non-coronary intensive care units (8). The age and gender adjusted incidence of severe sepsis lies around 300 cases per 100,000 inhabitants with an overall hospital mortality of close to 30% (8). A German investigation of 11,883 patients of 113 ICUs at 95 hospitals reports 1,503 cases (12.6%) with severe sepsis or septic shock (5). From their data the authors

[1] µg/kg/min

calculate an incidence rate of 11.64 per 1,000 ICU days for severe sepsis and septic shock. Moreover, they report a mortality rate of 34% in patients with severe sepsis/septic shock compared to a mortality rate of 6% in cases without sepsis (5). As such sepsis is a major risk factor for ICU mortality.

Pathophysiology of Sepsis

As per definition sepsis is an over exaggerated immune response of the host to a localized or generalized infection. During daily life the host is constantly confronted with potentially pathogenic germs. If one of these passes the physiologic barriers (for instance the gut barrier or the skin) it triggers an inflammatory response. In this situation the innate immune system is the first unspecific response to confront the invader. It consists of granulocytes, macrophages and natural killer cells as well as the complement system and cytokines. Regarding the cytokines, pro-inflammatory mediators such as interleukins (IL) 1, 4, 6, 8 (and others), interferon gamma (INF-γ) and tumor necrosis factor alpha (TNF-α) are opposed by anti-inflammatory cytokines such as IL-10 or transforming growth factor beta (TGF-β). Tissue damage occurs, if inflammatory and anti-inflammatory response are uncoupled or if there is an excessive inflammation (9). The initially local process may spread throughout the body leading to leaky vessels and activation of the coagulation cascade resulting in worsening of the microcirculation causing further organ damage (9-11). Regarding microcirculation the abdominal organs (splanchnic region) receive 25-35% (maximum in phases of digestion) of the cardiac output (12, 13). In scenarios with intestinal hypo-perfusion the gut turns into a toxic organ releasing pro-inflammatory cytokines (14). This results in systemic vasodilation, increased capillary leakage, decreased venous return and consequently reduced cardiac output with impaired tissue perfusion (15, 16). As a

reaction the body tries to centralize the blood volume to support the essential organs heart, brain and lungs. This can be (at least temporarily) achieved by activation of the renin-angiotensin-aldosterone-system and the secretion of other vasoactive substances. All of this leads to a further decrease of intestinal perfusion with increasing hypoxia and consequent disruption of the gut barrier (17).

Gut barrier

The gut barrier is one of the most important barriers of the human body. It functions as selective filter allowing passage of water, nutrients and gases and at the same time serves as barrier for bacteria and their toxic metabolites (18). The gut barrier is constituted by an inner mucus layer followed by the intestinal epithelial cells. The total surface area of the intestinal epithelium lies somewhere around 30m^2 equaling about half a badminton court (19). In the small intestine these epithelia are structured into villi (0.2-1mm), crypts and microvilli. Epithelial protuberances (lamina epithelialis) and the lamina propria form the villi. Most of all cells at the villus border are enterocytes with a surface enlargement by microvilli responsible for digestion and absorption on their apical side (20).

The stem cells, which are responsible for the renewal of the intestinal epithelial cells (IECs) lie within the crypts. IECs are classified into Paneth cells, normal intestinal epithelium and goblet cells.

Paneth cells are located in the crypts and can produce and secrete antimicrobial peptides like defensins and lysozymes that are toxic to bacteria (21-23).

The “healthy” intestinal epithelial cells are interconnected by a junctional complex consisting of tight junctions (TJs, zonulae occludentes) on the luminal side forming para-cellular seals to prevent the flux of hydrophilic molecules (20). Further along the

line adherens junctions (AJs), including zonulae and fasciae adhaerentes, (intermediate junctions) and maculae adhaerentes (DES, desmosomes) towards the apical side are known to determine the cellular polarity and regulate the cell-cell communication. Gap junctions (nexus) are dispersed all over the contact area of epithelial cells to ensure the exchange of substances between two adjacent cells (24, 25). Histologically the positions of all four forms of symmetrical junctions are mostly not at random but under developmental and functional control so that disorder often leads to disease (24, 26).

The IECs originate from the stem cells in the crypts and then migrate towards the tip of the microvilli where they die due to apoptosis within a life span of 4-5 days and are shed to the intestinal lumen (27). One single crypt produces 300 to 400 cells per day (23). In addition to the transport of nutrients they can modify the TJ structure and produce pro-inflammatory cytokines and reactive oxygen species as response to pathogens or metabolic stress (25). Among the cellular connections the tight junctions take a major part in supporting the epithelial integrity.

TJs are composed of different substructures including tight junction protein-1 (TJP-1), occludin (OCLN) and claudins (CLDN). Occludin with a molecular weight of 65 kD is a protein with four transmembrane areas and two extracellular loops (28). As OCLN-deficient mice show no significant disturbance of structure or function of TJs, the definitive function of occludin is still unclear (29). Different claudins have been described throughout the human body (30). They have a molecular mass of 20-27 kD and consist of four transmembrane helices with two extracellular loops (28). By implementing different claudins from their cytoplasmatic storage site to the TJ the IECs are able to influence the para-cellular permeability (31). There are some claudins which increase (2 and 10) and others which decrease (1, 3, 8 and 15) para-cellular permeability (26, 32).

Goblet cells which occur in a smaller number in the small intestine compared to the large intestine in the villi produce mucus, which is a very important component of the gut barrier. The small intestine is covered by a single, and the large intestine by a double layer of mucus (33-35). The mucus contains soluble glycoproteins termed mucins, which are capable of binding water molecules (36). The luminal layer of the small intestinal mucus is predominantly formed by mucin-2 (MUC-2) (33, 34). Additional protection is provided by a carbohydrate-rich glycocalyx composed of glycoproteins as transmembrane mucins (37). In humans MUC-13 and MUC-17 are the most important in the maintenance of mucosal homeostasis, mainly by limiting the contact between pathogens and the mucosa (38, 39). The factors contributing to an intact gut barrier are summarized in FIGURE 1.

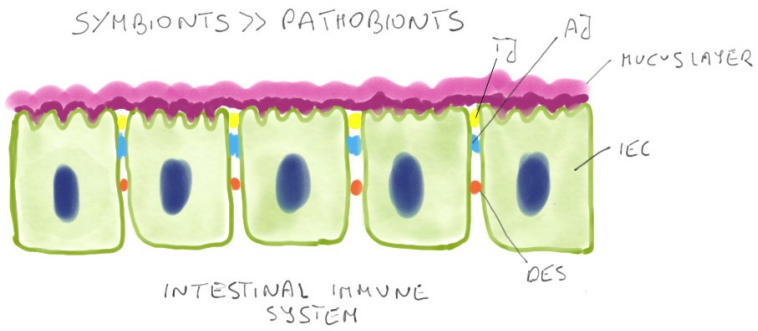

Figure 1: Factors contributing to an intact gut barrier. TJ…tight junction; AJ…adherens junction; IEC…intestinal epithelial cell; DES…desmosome.

The intestinal epithelium has a histologically specific appearance in every section of the gut. The jejunum compared to the ileum has a thick and heavy wall with simple arcades forming few large loops in mesentery and a larger diameter. It is characterized by the appearance of large, tall and closely packed plicae circulares and numerous villi. It contains a higher number of thicker folds then the ileum. The characteristics of the ileum are thin and light walls with complicated arcades forming

many short loops in the mesentery and contain many lymphoid follicles (Peyers patches). It is smaller in diameter than the jejunum and low and sparse plicae circulares can be found. The plicae circulares are completely absent in the distal part of the ileum (23, 40).

The histology of the colon shows no villi like the small intestine. The colon mucosa borders crypts of Lieberkühn populated by a high proportion of goblet cells with a flat inter-cryptal surface epithelium. Hardly any Paneth cells can be detected in this bowel segment (41).

Pathways of Intestinal Substance Uptake

There are two different pathways for substance uptake in the small intestine (42): the trans-cellular pathway and the para-cellular pathway.

The trans-cellular pathway allows substances to pass through the IEC. The lipid bilayer of the cellular wall is permeable for lipophilic and impermeable for hydrophilic compounds. Therefore, IEC carry a special transporter mechanism for essential water soluble substances (28).

The para-cellular pathway is the second possibility for diffusion or osmosis, but also for restricted uptake of selected substances between the enterocytes (43). This pathway depends on the status of the junctional complex linking the IECs (see description above). There are two different possibilities for para-cellular selective transport (FIGURE 2):

1.) The pore pathway is regulated by the TJ protein composition (mainly by implementing different types of claudins). It allows a passage of solutes with a diameter < 4 Angström (28).

2.) The leak pathway allows passage of larger molecules and is caused by temporary breaks in the TJ complex and linked to contractions of the actomyosin ring causing (MLCK mediated) dilation of the TJ (28, 44, 45).

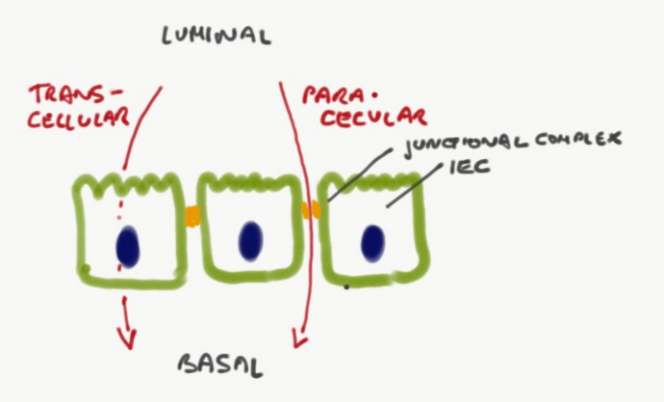

Figure 2: Trans- and paracellular transport at the intestinal barrier.

Alterations of Gut Barrier in Sepsis

In severe illness, for an example in sepsis, various factors can lead to disruption of the intestinal barrier: Breakdown of the mucus layer, increased para-cellular permeability (alteration of TJ porosity, or opening of TJ, AJ and desmosomes), loss of enterocyte integrity (necrosis or apoptosis of IECs), decreased intestinal immunity and/or altered intestinal microbiome (with dominance of pathobionts) (FIGURE 3; reviewed in (27) and (39)). This breakdown can be triggered by a broad variety of inflammatory factors as IL-1β (46, 47), IL-4 (48), IL-6 (49), TNF (50, 51), INF-γ (52, 53), nitric oxide (54) and inflammatory prostanoids (55, 56); each of them increasing gut barrier permeability in vitro or in vivo (57).

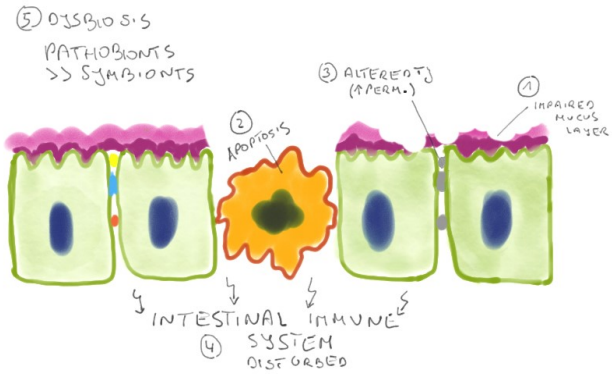

Figure 3: Factors causing a disruption of the intestinal barrier.

In this setting either bacteria or bacteria derived pathogen-associated-molecular-patterns (PAMPs) can pass the intestinal barrier further fueling the host´s inflammatory process. As such PAMPs like lipopolysaccharide (LPS), peptidoglycan or flagellin may bind to Toll-like receptors (TLRs) – predominantly TLR-4 - causing activation of macrophages. In consequence, activated macrophages produce and secrete pro-inflammatory cytokines as IL-1, INF-γ and TNF-α increasing the host´s inflammatory tone (58).

Furthermore, increased TNF-α levels directly influence the para-cellular permeability via their claudin composition. A possible mechanism for this is a nucleus factor kappa b (NFkB)-driven reduced expression of claudins 1, 3, 4, 5, 7, and 8 paired with increased expression of claudin 2 resulting in increased TJ permeability (26, 39, 59, 60). At the same time endotoxemia may result in a disrupted ultrastructure of occludin and zonulin-1 (ZO-1) further increasing para-cellular permeability (61). In contrast, anti-inflammatory cytokines like TGF-β and IL-10 result in activation of SMAD and SNAIL cascades causing increased expression of claudins 1, 3, 4 and 11 tightening TJs and reducing permeability (26). Furthermore, pro-inflammatory cytokines can promote the expression of myosin light chain kinase (MLCK). This enzyme phosphorylates the myosin light chain causing contraction of the acto-myosin

skeleton resulting in opening of the tight junctions (62-64). Additionally to increased TJ porosity pro-inflammatory cytokines may also lead to an increased expression of MLCK (64).

Apoptosis plays a major role in sepsis induced gut barrier dysfunction. In animal sepsis models and human cadaver studies increased epithelial/lymphocyte apoptosis was the dominant histological finding (65). Possible mechanisms for this are overexpression of IL-1β-converting enzyme and/or decreased levels of anti-apoptotic Bcl-2 or absence of lung surfactant proteins SP-A and SP-D (66, 67).

Among the above factors sepsis is associated with enhanced mucosal layer permeability (68, 69). In this regard ischemia/reperfusion models have shown a loss of hydrophobicity as most likely cause for altered intestinal permeability (70). This may also be associated with the intestinal dysbiosis observed during shock. In case of sepsis, the intestinal microbiome shifts towards the phylum of Proteobacteria with a decrease of symbionts (Firmicutes and Bacteroidetes). A reduction of mucus-forming and anti-inflammatory *Faecalibaterium* has been observed (71) and may be a link between microbiome and mucus breakdown in sepsis. Of course, drugs such as proton pump inhibitors; histamin-2-receptor antagonists or antibiotics may aggravate the shift of the intestinal microbiome towards an increase of pathobionts.

Summary of Possibilities to Investigate the Gut Barrier in Sepsis Models

Functional Permeability by Fluorescence Isothiocyanat Dextran (FITC - Dextran)

FITC - Dextran is a substance that is resorbed from the intestine in only very limited amounts in case of a healthy gut. In case of increased gut permeability, it is transferred to the serum and can be detected by photometry (extinction at 485 nm and

535 nm). As such it has been used as functional parameter to observe gut permeability in various disease models with increased gut permeability (72, 73). All of these studies were characterized by increased gut permeability resulting in elevated serum FITC - Dextran levels compared to controls. Regarding the mode of FITC passage to the serum three pathways can be assumed:

1.) an increase of TJ porosity by implementation of a different type of claudins (see section gut barrier above)
2.) an alteration of the status of the tight junction (open or closed)
3.) a total disruption of the IEC by means of necrosis or apoptosis

Alterations of the TJ structure can result in pores of a size of up to 4 Angstrom, the modification of the status (open/closed) in pores with a size of up to 50 Angstrom. Depending on the structure FITC - Dextran has a diameter of >14 Angstrom. As such a para-cellular passage is only possible through altered TJ status (28). Finally, the serum FITC - Dextran levels give a global overview of the permeability of the entire intestine (unless segments have been surgically isolated), but not on the functionality of specific segments.

Evaluation of IEC Apoptosis

IEC apoptosis can be assessed by immune-histology. There are various techniques and markers, which have been described as a valid possibility to stain for apoptosis (HOECHST, TUNEL) (74, 75). Also the way of quantification is described very often in different ways and varies from lab to lab including discussions about the validity of this quantifications (76). Two possibilities are known for quantifying apoptosis:

On the one hand the number of apoptotic cells is set in relation to the number of non-apoptotic vital IECs as an apoptotic index or on the other hand the number of apoptotic cells is set in relation to the number of proliferating cells. Both ways are used and represent an accepted immuno-histologic marker (77, 78).

Furthermore, various proteins involved in the apoptotic process can be assesses either directly at the protein (ELISA) or at the gene expression level (PCR). In this regard, Bax, Bak, Caspase-3, Lamin B and Bad (among others) have been described as pro-apoptotic and Bcl-2 and Survivin as anti-apoptotic. A combination of these methods gives a detailed insight into IEC apoptosis in sepsis models (76, 77, 79).

Evaluation of Tight Junctions

As already described above TJs are amongst the most important structures for the integrity of the intestinal barrier. TJs can be affected by either a change of their porosity or their status (open or closed).

In case of sepsis various mechanisms lead to implementation of claudins (for instance claudin 2) with an increased porosity and consequently increased para-cellular leakage. The porosity can be assessed by determining the transmembrane potential difference of bowel samples in experimental settings (28). The claudins and other TJ components can be examined directly, either on the protein level with ELISAs or on the gene expression level by PCR.

The status of the tight junction is difficult to capture. In this regard histological examinations can help to detect increased intercellular spaces which can be further specified by transmission electron microscopy (TEM) (FIGURE 4). Additionally, the

MLCK as key regulator of the acto-myosin contraction and thus the TJ status can be evaluated on the gene expression or protein level.

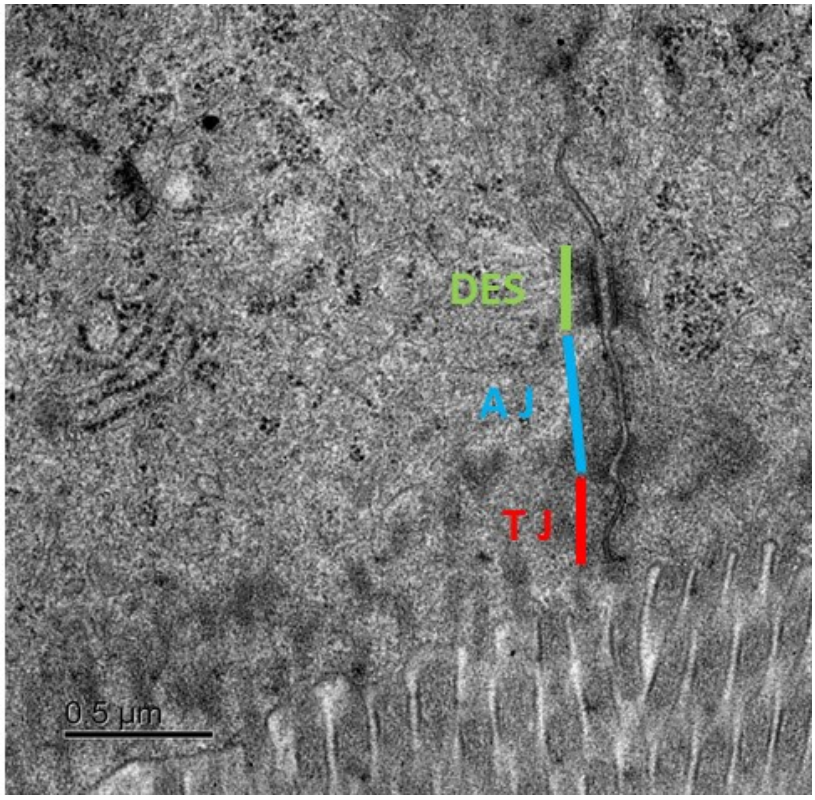

Figure 4: Determination of a desmosome (DES), an adherens junction (AJ) and a tight junction (TJ) at a cell-cell contact with TEM

Examination of the Mucus Layer

As described above, the mucus layer is an essential component of the gut barrier. Histological sections of different gut sections with H&E or other staining methods may also be used to directly measure the mucus thickness although it is not common (80). If repeated within the same section and in different sections it can give a good first impression on the mucus production in small and large intestine (81). Furthermore, mucus components (as for instance MUC-2 as major component of the

luminal mucus and MUC-17 as transmembrane component of the apical portion and part of the glycocalyx) can be targeted by immune-histology, ELISA or PCR (37).

Vitality Markers of IECs

Vital IECs are the main source of citrulline, an amino acid which is produced by the IEC mitochondria of mature enterocytes at the upper part of the villi (27). Citrulline is released to the portal system, passes the liver and is then captured by the kidneys. Here it is metabolized to arginine, which is again released to the plasma (27). As such, plasma citrulline levels are a marker for the vitality of IECs – a larger number of vital IECs result in higher citrulline levels (82). In this regard plasma concentrations between 20-60µmol/l have been reported for healthy adults in Western countries (83).

Furthermore, IECs contain intestinal free fatty acid binding protein (I-FABP) in their cytoplasm. In case of IEC disruption, I-FABP is released to the serum und can be detected as a measurement of IEC disturbance (high levels reflect enterocyte destruction). In human studies plasma levels of > 100 pg/ml were associated with enterocyte destruction (84, 85).

Small Angle X-Ray Scattering (SAXS)

Many research projects in the past have focused on the investigation of the gut barrier applying various methods. Amongst others, the permeability for fluorescence isothiocyanate dextran (FITC-dextrane), electron microscopy, conventional histology, immunohistochemistry and quantitative analysis of tight junction components have been described (72, 73). However, none of these techniques can offer detailed information about the ultrastructure of IECs. Small-angle X-ray scattering (SAXS) is a

non-destructive experimental method used for ultrastructure analysis in materials sciences (86). A sample is hit by an x-ray beam and while the major part of this beam passes the sample unperturbed, a small proportion is scattered at zones of different densities – for instance the border between lipid bilayers and the cytosol (87) (FIGURE 5).

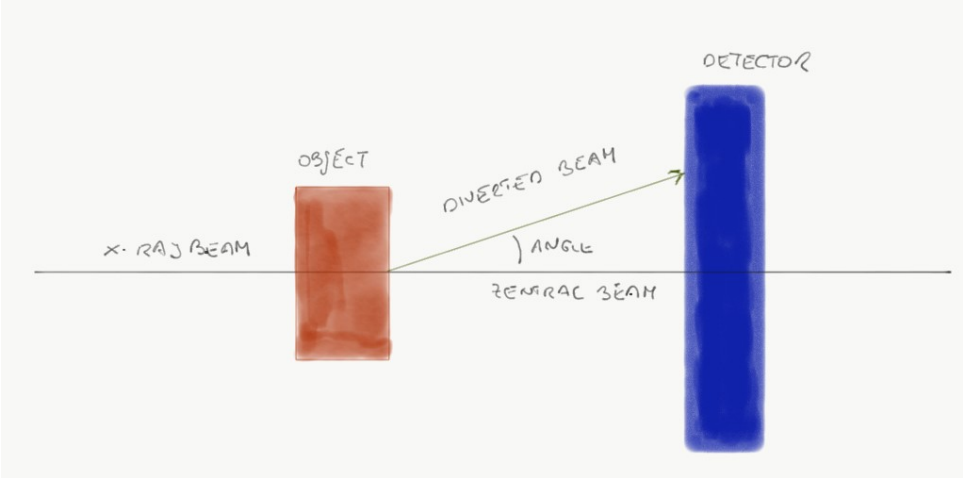

Figure 5: Theoretical set-up of SAXS measurements.

Presently, SAXS has been used to study a variety of biological materials (88-91) including soft tissues (86, 91-93). However, until now SAXS has not been used to assess nano-structural alterations of the bowel wall during sepsis.

Aim of the Study

It was the aim of this experimental study to apply a combination of material characterization techniques such as SAXS, light and electron microscopy to study the ultrastructure of the bowel wall in the early phase of sepsis. Additionally, we sought to investigate mechanisms (status and composition of tight junctions, epithelial apoptosis and altered cellular architecture) leading to gut hyper-permeability in a murine model of early sepsis.

Material and Methods

All described methods were carried out in accordance with relevant guidelines and regulations and were approved by the veterinary board (Austrian Federal Ministry of Education, Science and Research, BMWFW 66.010/0028-WF/V/3B/2017).

Eighteen male C57Bl/6 mice were obtained from Harlan Laboratories at an age of 7 weeks. After delivery, mice were numbered and accustomed to the new surroundings for 1 week. All animals were housed in groups up to 5 animals and provided with nesting material as enrichment. The animals had free access to chow and water at all times and were subjected to a 12h light-dark cycle. After 1 week of acclimatization the animals were split into two groups by weight equalized for average weight and standard deviation. All animals were kept under the same housing conditions and in the same rack. Mice of both groups were gavage fed with 500mg/kg FITC-dextrane 4SD (size 14 Angstrom; Sigma Aldrich Handels GmbH, Vienna, Austria) dissolved in PBS at 50mg/ml. Thirty minutes after gavage animals of the sepsis group (n=10) were anesthetized with 0.05mg/kg fentanyl, 5mg/kg midazolam and 0.5mg/kg medetomedine intra-peritonially. Under temperature control by using a heating mat (TempControl II; 908100-2; TSE Systems, Germany) all mice of both groups were shaved and the skin disinfected. Mice of the sepsis group received a median laparotomy and cecal ligation and puncture (CLP) was performed (FIGURE 6). Briefly, the cecum was mobilized, ligated and punctured with a 20G needle as described before (94). After wound closure in double layers anesthesia was antagonized with 2.5mg/kg atipamezole and 0.5mg/kg flumazenil. Animals of the control group (n=8) underwent sham operation consisting of general anesthesia as described above, median laparotomy, exteriorization and replacement of the cecum

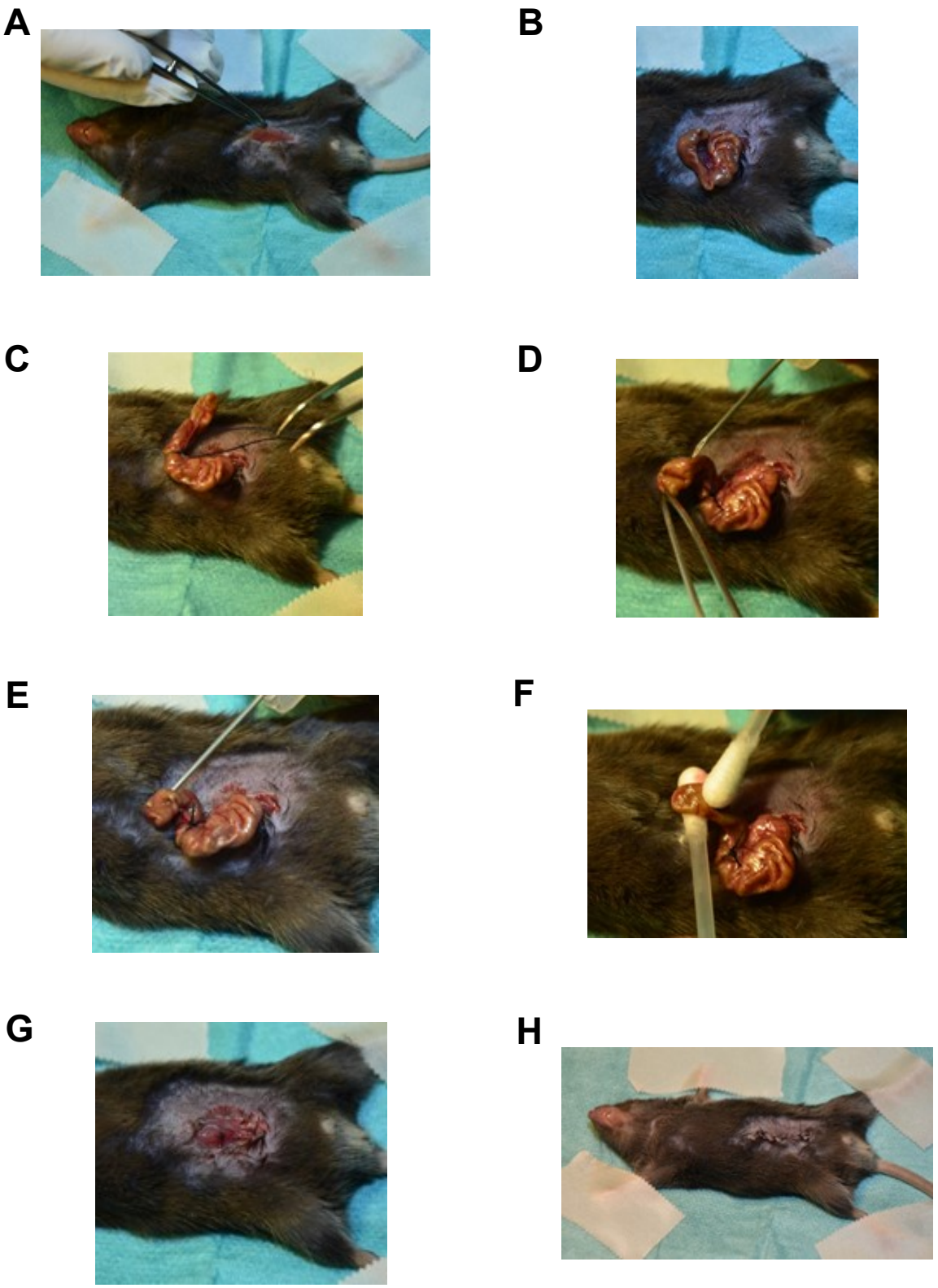

Figure 6: Execution of a CLP; Opening of the abdominal cavity (A); Excavation of the cecum (B); Ligature of the cecum (C); Puncture of the cecum (D, E); Release of cecum content (F); Closure of the peritoneum (G) and the skin (H)

and abdominal closure in double layers. Postoperatively, animals of both groups received 0.1mg/kg subcutaneous buprenorphine as pain therapy and 1 hour after complete recovery from anesthesia 400µl subcutaneous NaCl as water depot. Behavior of the animals was constantly monitored for severe pain or adverse events using a standardized scoring system as required by the governmental veterinary board (SUPPLEMENT 1). Eight and a half hours after FITC-Dextrane gavage mice were re-anesthetized with the same anesthesia mix as described above. After opening the chest the heart was punctured with a 23G needle and as much blood as possible was harvested. Mice were then immediately sacrificed by cranio-cervical dislocation. The abdomen was opened to dissect 4cm of terminal ileum (starting 1cm orally of the ileo-cecal valve), 4cm of the proximal jejunum and 4cm of colon (starting 1cm caudally of the ileocecal valve). The different gut section dissections of jejunum, ileum and colon were parted into the following samples each for further procedure in this order: H&E staining, ELMI, ELMI reserve, SAXS.

Inflammatory Cytokines

Pro-inflammatory cytokines were determined with a Millipore Merck Luminex® Kit (MMHMAG-70K, Merck Chemicals and Life Science GmbH, Vienna, Austria) which was customized for Interleukin (IL)-1α, IL-1β, IL-6, Tumor Necrosis Factor (TNF)-α and Interferon (INF)-γ. According to the manufacturer´s instruction all serum samples were diluted 1:2 in the provided assay buffer after complete thawing from -80°C. After completing the immunoassay procedure as described in the manual (as overnight protocol) all standards, controls and pro-inflammatory cytokines were measured at the

same time as duplicates for all samples immediately after preparation with a Bio-Plex® 200 (BioRad, Germany).

FITC-Dextrane Assay for Gut Permeability

After clotting for 30 minutes, the whole amount of blood was centrifuged for 10 minutes at 10,000rpm. 150µl of the supernatant serum were stored in absolute dark at 4°C until measurement. The serum FITC-Dextrane content was determined fluorometrically at wavelengths of 485nm and 535nm as described in the manufacturer's instructions. The rest of the supernatant serum was aliquoted, snap frozen and stored at -80°C for further investigation. After the measurement the used serum was put into Eppendorf tubes again, marked and stored at -80°C as reserve.

Light Microscopy of Jejunum, Ileum and Colon Samples

Ileum, jejunum and colon samples underwent standard histological work-up with fixation, dehydration, embedding, cutting, rehydration followed by hematoxylin-eosin staining. The H&E staining was conducted with a SAKURA DRS 2000 slide stainer (SAKURA Finetek, USA) according to the protocol shown in TABLE 2. Afterwards, the colored slides were covered with glass mounting medium (Tissue Tek, Sakura, Finetek, USA).

Histological examination for bowel wall inflammation was conducted from three slices per ileum, jejunum and colon sample in three different magnifications (100x, 200x and 400x) with an Olympus DP71 camera connected to an Olympus BX51

microscope. The measurements included the determination of villus height, crypt depth, villus:crypt ratio, lymphocytes per 100 enterocytes and bowel wall inflammation according to a modified Marsh-Oberhuber classification (FIGURE 7) (95). Additionally, the height of the upfolding in colon samples was determined with ImageJ.Ink 1.52® in hematoxylin-eosin stains of three colon samples per mouse with a 10x objective lens as well as the width of the intercellular spaces in ileum samples was determined with ImageJ.Ink 1.52® in hematoxylin-eosin stains of three ileum samples per mouse with a 100x oil immersion objective lens (FIGURE 8).

Table 2: Protocol of the automated H&E staining with the SAKURA DRS 2000 slide stainer (SAKURA Finetek, USA)

Step	Station	Reagents	Time	Automated Mixing
1	S	Start station	2min	
2	25	Xylol (all times: Merck Chemicals and Life Science GmbH, Vienna, Austria)	2min	yes
3	24	Xylol	2min	yes
4	23	EtOH abs./Xylol (all times: Merck Chemicals and Life Science GmbH, Vienna, Austria)	2min	yes
5	5	EtOH abs. (all times: Merck Chemicals and Life Science GmbH, Vienna, Austria)	2min	yes
6	6	EtOH abs.	2min	yes
7	3	EtOH 70%	2min	no
8	2	EtOH 50%	2min	no
9	7	Aqua dest.	2min	yes
10	9	Hämalaun (Merck Chemicals and Life Science GmbH, Vienna, Austria)	1min	yes
11	Wash	Water	1min	yes
12	Wash	Water	1min	yes
13	20	Eosin-Phloxin (Internal pharmacy)	2min	yes
14	7	Aqua dest.	2min	no
15	2	EtOH 50%	1min	no
16	3	EtOH 70%	1min	no
17	19	EtOH abs.	2min	yes
18	18	EtOH abs.	2min	yes
19	17	EtOH abs./Xylol	2min	yes
20	16	Xylol	2min	yes
21	E	End		

Table 3: modified Marsh-Oberhuber classification, modified according to Adelman 2018 (95)

Grade	Description and components
0	Normal - Normal appearing mucosal and villi architecture
I	Infiltrative - Normal to slightly changed mucosal and villi architecture; increased numbers of IELs
II	Hyperplastic - Normal to slightly changed mucosal and villi architecture; enlarged crypts and increased crypt cell division; increased numbers of IELs
IIIA	Partial villus atrophy – shortened, blunt villi; mild lymphocyte infiltration, enlarged hyperplastic crypts
IIIB	Subtotal villus atrophy – clearly atrophic villi, enlarged crypts, increased rate of immature epithelial cells, influx of inflammatory cells
IIIC	Hypoplastic – total villus atrophy, loss of villi, severe crypt hyperblasia, infiltrative inflammatory lesion

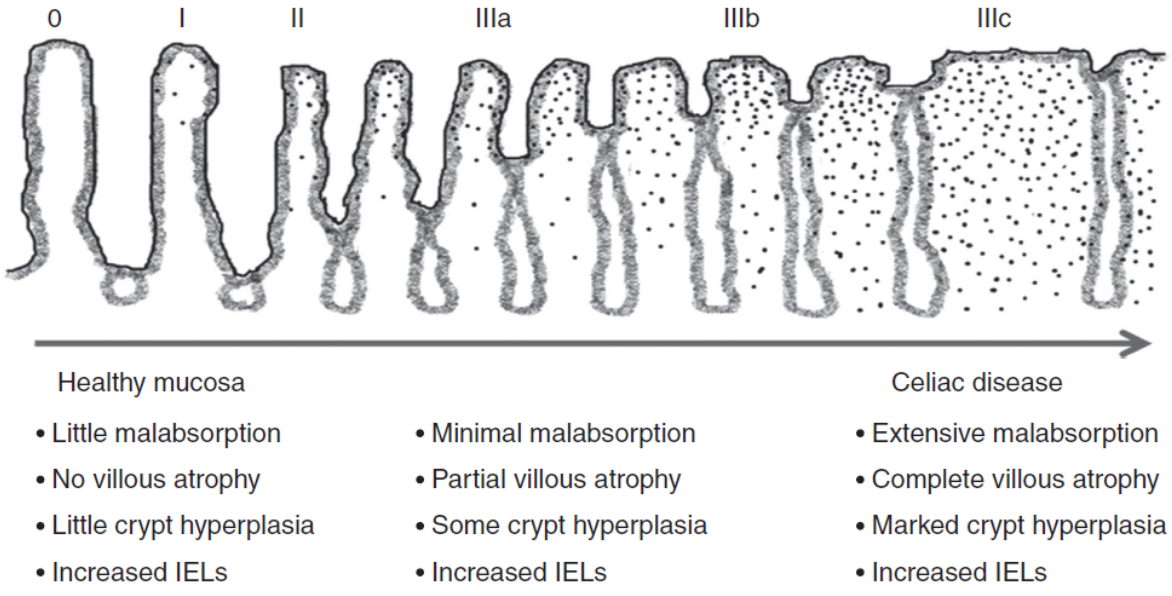

Figure 7: Schematic depiction of Marsh-Oberhuber grades 0-IIIC as described in Table 3 according to Adelman et al (95).

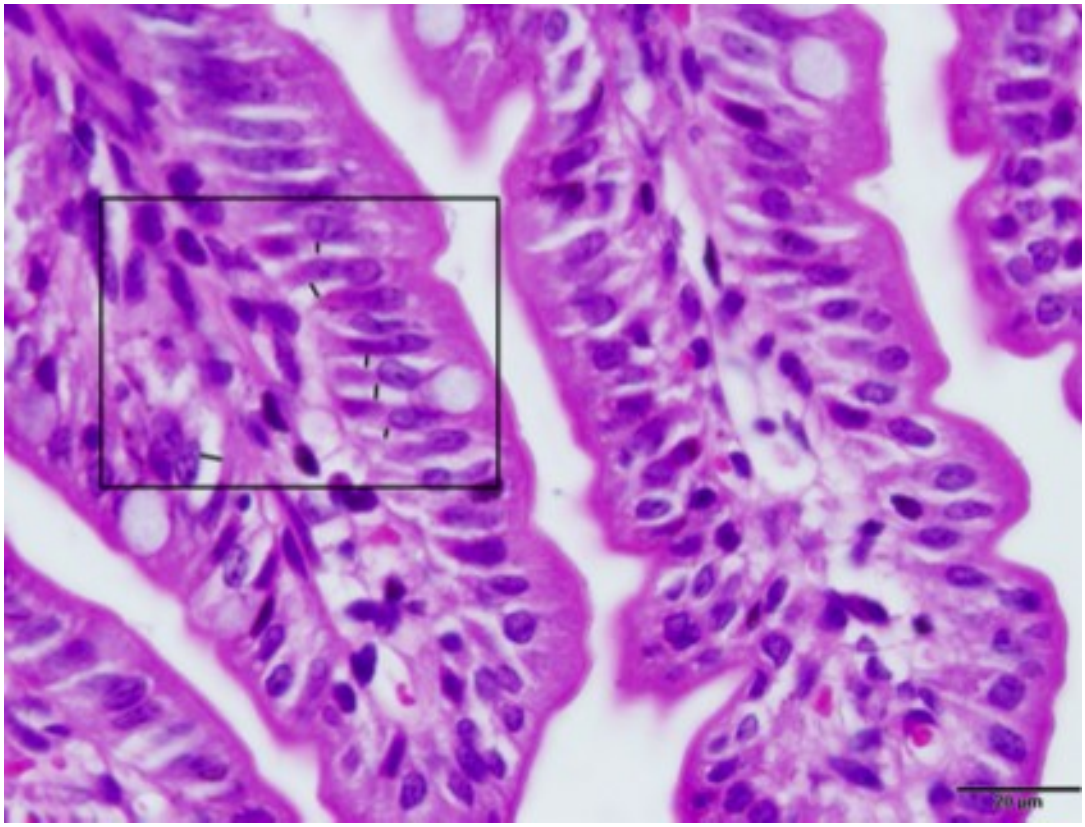

Figure 8: Determination of the intercellular distance. H&E staining, magnification 100x (oil immersion lens).

For a possible detection of 'pale' cells (FIGURE 9) a Toluidin blue staining of three 5µm paraffin slices (Thermo Scientific Microtome HM3555) per ileum was performed as described in TABLE 4 and evaluated with photos taken with an Olympus DP71 camera connected with an Olympus BX51 microscope with a 100x oil immersion objective lens.

Table 4: Protocol of the Toludin blue staining

Step	Reagents	Time
1	Xylol (all times: Merck Chemicals and Life Science GmbH, Vienna, Austria)	5min
2	Xylol	5min
3	EtOH abs. (all times: Merck Chemicals and Life Science GmbH, Vienna, Austria)	5min
4	EtOH 90%	5min
5	EtOH 70%	5min
6	EtOH 50%	5min
7	Aqua dest.	3min
8	Aqua dest.	3min
9	Aqua dest.	1min
10	Toluidin blue solution (filtrated 0,1% solution, Certistain C.I.52040)	5min
11	Aqua bidest.	1min
12	Aqua bidest.	1min
13	EtOH 90%	1min
14	EtOH abs.	1min
15	Xylol	1min
16	Xylol	mount
	Cover with 1 drop glass mounting medium (Tissue Tek, Sakura, USA) and cover slip	

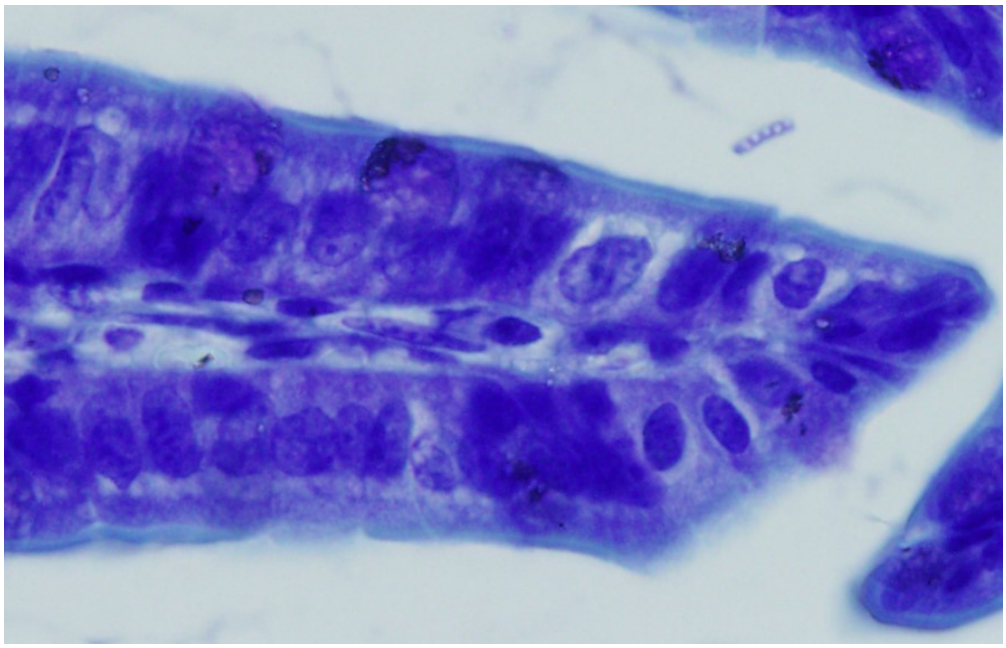

Figure 9: weakly stained ('pale') cells (toluidine blue staining; 400x oil immersion).

Conventional Scanning Electron Microscopy (CSEM)

SEM analysis were conducted by a partner at the Institute of Material Sciences at the University of Natural Resources and Life Sciences in Vienna. Of each animal one piece of ileum and one piece of colon were opened on the anti-mesenteric side. The bowel content was removed by careful rinsing with physiologic saline solution. Samples were then fixed with 5% buffered glutaraldehyde at 4°C for 2h. After fixation with 1% osmiumtetroxide samples were dehydrated in an ascending alcohol series. The dehydrated specimens were bathed in 1,1,1,3,3,3-hexamethyldisilazane and gold coated with an Edwards Scancode Six® (Hind High Vacuum Company Private Limited, Bangalore, India) for 2 minutes. SEM was conducted with a Quanta FEG 250® (Thermo Fisher Scientific) electron microscope using a 20kV beam. Images were taken with xTm 4.1.7.2095® (Thermo Fisher Scientific). Three images from tilting angles of -5°, 0° and 5° were obtained at a magnification of 1,000x and used for 3D reconstruction with MeX 5.1® (Alicona Imaging GmbH, Raaba, Austria). From 125 x 200µm areas of these 3D reconstructions the surface roughness (R_a) was calculated using a cut-off wavelength of 30µm.

Transmission Electron Microscopy (TEM)

Similar to SEM, one cm of ileum and one cm of colon were prepared for TEM analysis. Specimens were fixed in in 2.5% (wt/vol) glutaraldehyde and 2% (wt/vol) paraformaldehyde in 0.1M phosphate buffer, pH 7.4, for 2h, postfixed in 2% (wt/vol) osmium tetroxide for 2h at room temperature. After dehydration (dehydrated in graded series of ethanol), tissues were infiltrated (ethanol and agar 100 epoxy resin, pure agar

100 epoxy resin) and placed in agar 100 epoxy resin (8h), transferred into embedding molds, and polymerized (48h at 60 °C). Ultrathin sections (70nm) were cut with a UC 7 Ultramicrotome (Leica Microsystems, Vienna, Austria) and stained with lead citrate for 5min and platin blue for 15min. Images were taken at 120kV with a Tecnai G 2 FEI microscope equipped with an ultrascan 1,000 ccd camera (Gatan). The images were examined for average number of microvilli, widening of the intercellular contacts at the level of the TJ, the adherens junction and the desmosomes. Measurements were conducted with ImageJ.Ink version 1.52® at the widest spot each for at least 10 cell-cell contacts per animal (FIGURE 10).

Figure 10: Determination of the intercellular distance at the level of the tight junction (TJ), adherens junction (AJ) and desmosome (Des).

Fluorescence Immunohistochemistry for IEC Apoptosis

HOECHST staining was performed to determine the ratio of apoptotic intestinal epithelial cells of the ileal sections. Fixation and paraffin embedding was performed according to standard histological procedures. 2.5µm thick paraffin slices were submersed in Roticlear solution (Carl Roth GmbH + Co. KG, Karlsruhe, Germany) followed by 2x 100% ethanol, 70% ethanol, 50% ethanol, distilled water and PBS for 5 minutes each. A HOECHST working solution was prepared by diluting 25mg original medium (HOECHST B2261-25MG, Lot 017K4122, Sigma Aldrich Handels GmbH, Vienna, Austria) to a concentration of 5µg/ml with distilled water (the HOECHST solution has an absorption frequency of 350nm and an extinction frequency of 461nm). Samples were transferred to Hoechst working solution (at a concentration of 5µg/ml for 10 minutes in absolute darkness). The slices were then washed in PBS three times, transferred to Superfrost Plus® slides (Thermo Fisher Scientific), covered with Vectashield® Mounting Medium (Vector Laboratories LTD, Peterborough, UK) and Menzel coverslips (Gerhard Menzel GmbH, Braunschweig, Germany). Microscopy was performed with an Olympus BX51 fluorescence microscope with an Olympus DP71 camera using a cell sens standard program. A grey-scale photo was taken and the histogram adjusted to 10-125. False color images were obtained in green and red for further examination. Two representative regions were selected for each specimen and 2 specimens per mouse were evaluated at an enlargement of 200x (about 150 enterocytes/field). The apoptotic cell ratio was determined as percentage of apoptotic nuclei in relation to the total number of enterocytes.

RNA Gene Expression of Tight Junction and Apoptosis Proteins

Quantitative real time PCR for gut permeability was performed in ileum sections. Markers (tight junction protein 1, occludin-1, claudin 2 and claudin 4) were chosen according to previous reports in the literature (96). Total RNA from frozen mouse ileum segments was isolated with a Qiagen miRNeasy Micro Kit (Qiagen, Hilden, Germany) with DNAse treatment (Qiagen, Hilden, Germany) according to manufacturer's instructions. RNA yield was quantified on a NanoDrop 2000c spectrophotometer. For reverse transcription 1µg of total RNA was used in the High Capacity cDNA Reverse Transcription Kit (Thermo Fisher Scientific) according to manufacturer's instructions. The cDNA was used as template for quantitative RT-PCR reactions in a BioRad CFX 384 real-time PCR detection system with the assays β-actin (Actb; Mm00607939_s1), hydroxymethylbilane (Hmbs; Mm01143545_m1) as housekeeping genes. Tight-junction-protein-1 (TJP-1; Mm00493699_m1), occludin-1 (OCLDN-1; Mm00500912_m1), claudin 4 (CLDN-4; Mm00515514_s1) and claudin 2 (CLDN-2; Mm00516703_s1) were selected for tight junction evaluation. Additionally, Bax (Bax; Mm00432051_m1), Bad (Bad; Mm00432042_m1), Caspase 3 (Casp3; Mm0195085_m1), Lamin B1 (Lmnb1; Mm0521949_m1), Bak1 (Bak1; Mm00432045_m1) and Bcl2 (Bcl2; Mm00477631_m1) were chosen for characterization of apoptosis (Thermo Fisher Scientific).

Briefly, in 10µl reactions 4µl cDNA were used in triplicates in a PCR reaction with 5µl TaqMan Genexpression MasterMix (Thermo Fisher Scientific), 0.5µl assay and 0.5µl dH2O. Cycling conditions were of initial UDG incubation at 50°C for 2 minutes, enzyme activation at 95°C for 10 seconds followed by 40 cycles of

denaturation at 95°C for 15 seconds and annealing and extension at 60°C for one minute. β-actin and Hmbs genes were used as housekeeping genes for normalization.

Tight Junction Protein ELISA

Additionally to the PCR, an ELISA was conducted for claudin 2 (ABIN1745307; antikörperonline.com), claudin 4 (ABIN1745294; antikörperonline.com), occludin-1 (ABIN773507; antikörperonline.com) and zonulin (MBS748504; MyBioSource.com). Measurements of claudin 2, claudin 4 and occludin were conducted from tissue homogenates of well cleaned ileum samples produced with an Ultra Turrax T25 digital (Ika, Germany). Zonulin measurement was conducted with diluted serum samples (1:2 or 1:4). The ELISA Kits (BlueGene Biotech, Shanghai; MyBioSource, USA) were operated according to the manufacturer's instructions which were identical for claudin 2, claudin 4, occludin and zonulin. The tissue homogenates or serum samples of the animals were single measured whereas all standards and the blank were measured as duplicates. After pipetting 100µl of either standard or blank or tissue homogenate into the provided 96-well plate according to the prior prepared loading scheme, 10µl of balance solution and 50µl of conjugate were well mixed with the fluids in each well plate slot. The plate was covered immediately afterwards and incubated at 37°C for 1 hour. 5 identical washing steps were conducted before 50µl of substrate A and 50µl of substrate B were added. All wells were covered immediately because of light sensitivity and incubated again at 37°C for a maximum of 30 minutes. 50µl of stop solution were mixed in the wells and the 96-well plates were immediately measured at 450nm with a Spectramax Plus 384 (Molecular Devices, LLC, USA).

Small-Angle X-Ray Scattering (SAXS)

Bowel segments for SAXS analysis (ileum and colon) were opened on the anti-mesenterial side immediately after harvesting. They were carefully rinsed with physiologic saline solution and bedded in Kallebrat foil (Kalle Austria GmbH, Guntramsdorf, Austria) (FIGURE 11). Samples were then shock frozen and stored at -80°C until measurement. For transport to the partner in Vienna specimen were stored on dry ice.

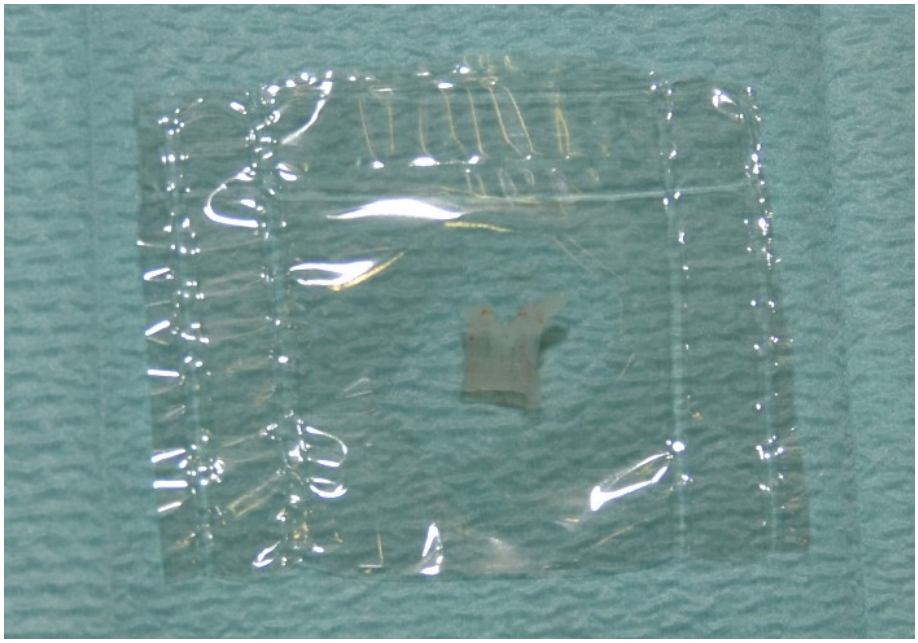

Figure 11: Piece of ileum applied to vacuum in Kalle Brat® foil

SAXS was performed by a partner at the Institute of Material Sciences at the University of Natural Resources and Life Sciences in Vienna. The detailed methods are copied from the original presentation in the following (97). For the SAXS measurements bowel samples of ileum and colon were opened and rinsed as described above. Gut samples were vacuum-sealed in Kalle Brat® foil (Ed. Haas Austria GmbH, Traun, Austria) and stored at -80°C. SAXS measurements were

obtained with a Rigaku S-MAX3000 SAXS System (Rigaku Europe SE, Neu Isenburg, Germany) with a Cu-α target Micro Focus X-ray tube MM-002+ (at a voltage of 45KeV and amperage of 0.88mA with an energy of 8.05KeV). The X-ray beam was focused through two diffraction-free germanium pinholes resulting in a beam diameter of 420µm at the sample. In order to preserve the structural integrity of the intestinal wall specimens were mounted on a temperature-controlled stage (HFS350X-CAP; Linkam Scientific Instruments, Tadworth, UK) and kept at a temperature of -21°C during the measurements. The detector – sample distance was 1,400mm allowing for a q-range of 0.01-0.6A^{-1}. The scattering vector q is related to the wavelength λ (λ = 1.54A) and the scattering angle 2θ.

$$q = \frac{4\pi}{\lambda} \cdot \sin\theta$$

Each measurement took 1,500 seconds and was carried out in vacuum conditions at a maximum pressure of 10^{-2}mbar to minimize absorption and diffraction by air. For measurements the direct beam was blocked with a 3.8mm beamstop and the scattering profile was recorded with a TRITON 200 2D multi wire gas-filled X-ray detector (Rigaku Europe SE, Neu Isenburg, Germany) with an active diameter of 200mm.

Since the bowel samples showed an isotropic scattering pattern indicating no preferred structural orientation in the sample, only the scattering intensity I was determined as a function of q.

For this purpose, the 2D scattering profiles were radially integrated and corrected by subtracting the background signal using SaxsGui 2.15.01® software packages. Scattering curves were then plotted as I(q) in a double logarithmic scale.

Distinct peaks observed at $0.1A^{-1}$ and $0.15A^{-1}$ were attributed to ice crystals due to blood remnants in the samples and excluded from the evaluation. The interpretation of SAXS data mainly focused on the low q range from 0.01 to $0.05A^{-1}$, which is attributed to structures in the size range of 12.5 to 62.8nm corresponding to potential alterations of tight junction nanopores. Since all plots showed straight lines in the regarded q range the evaluation was limited to fitting an exponential decay with an exponent describing the fractal dimension as described by Porod´s law (where D represents the scaling factor and α the Porod exponent.

$$I(q) = D \cdot q^{-\alpha}$$

This equation was implemented in a Python 2.7 script in order to evaluate the fractal dimensions of all samples.

The slope α of the double logarithmic Porod plot yields information about the fractal dimension of the scattering plot. Thus, a Porod exponent α = 1 is obtained from scattering by rigid rods, while α = 2 represents scattering from a flat (almost 2 dimensional) structure, such as lamellae or platelets, α = 4 characterizes smooth and a slope between 3 and 4 rough surfaces.

Statistics

Data was collected in Microsoft Excel 2016® spreadsheets. For statistical analysis data was transferred to SPSS 22.0®. Graphical imaging was performed with GraphPad Prism 7®. Nominal and ordinal data are displayed in numbers and percent, metric data as median and interquartile range (IQR). Comparisons of independent groups were conducted with Mann-Whitney-U-Tests. A Pearson test was performed to

search for correlations between different parameters. P values <0.05 were regarded as statistically significant differences.

Results

Clinical signs and serum cytokines

All animals survived to the defined end point. None of the animals exhibited severe pain necessitating early abortion of the experiment. Mice of the sepsis group had clinical signs of sepsis with higher post-operative sepsis scores compared to the control group (after sham operation) (FIGURE 12). A detailed overview of the different items of the clinical sepsis score is given in SUPPLEMENT 2.

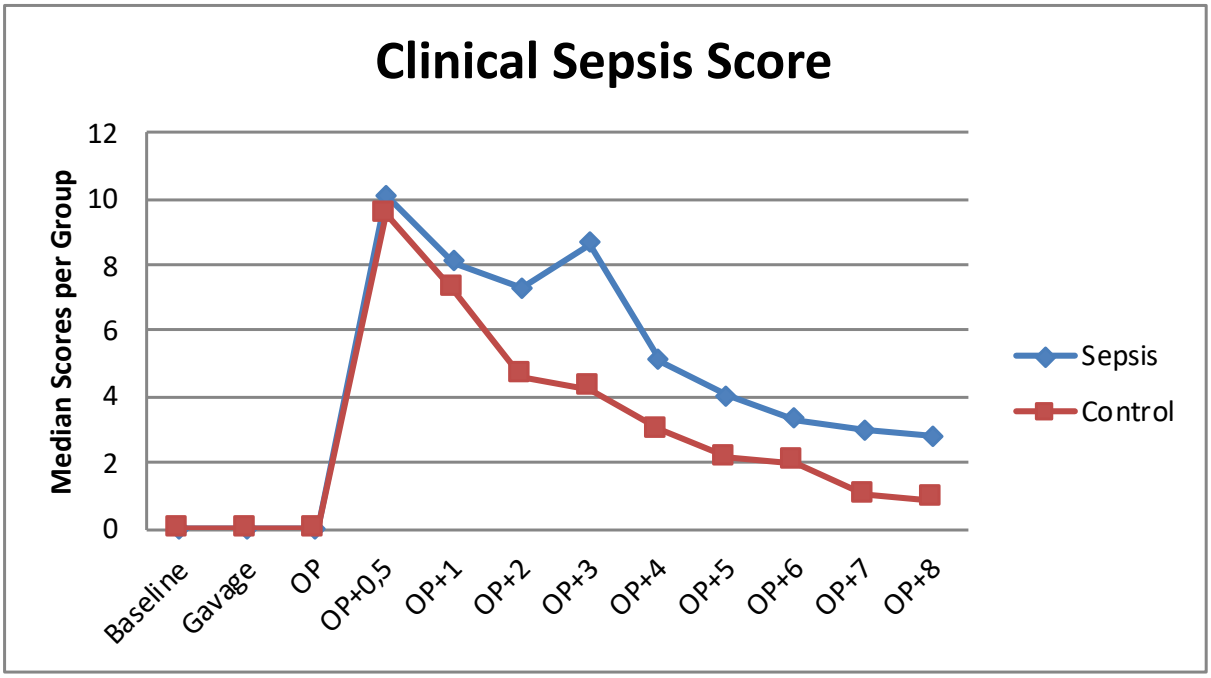

Figure 12: Total clinical sepsis score in the two study groups. Time in the time line on the x-axis is given in hours.

Septic animals exhibited significantly increased serum levels of the pro-inflammatory cytokines IL-1β, IL-6 and TNF-α verifying a septic condition. INF-γ and IL-1α were not changed (FIGURE 13).

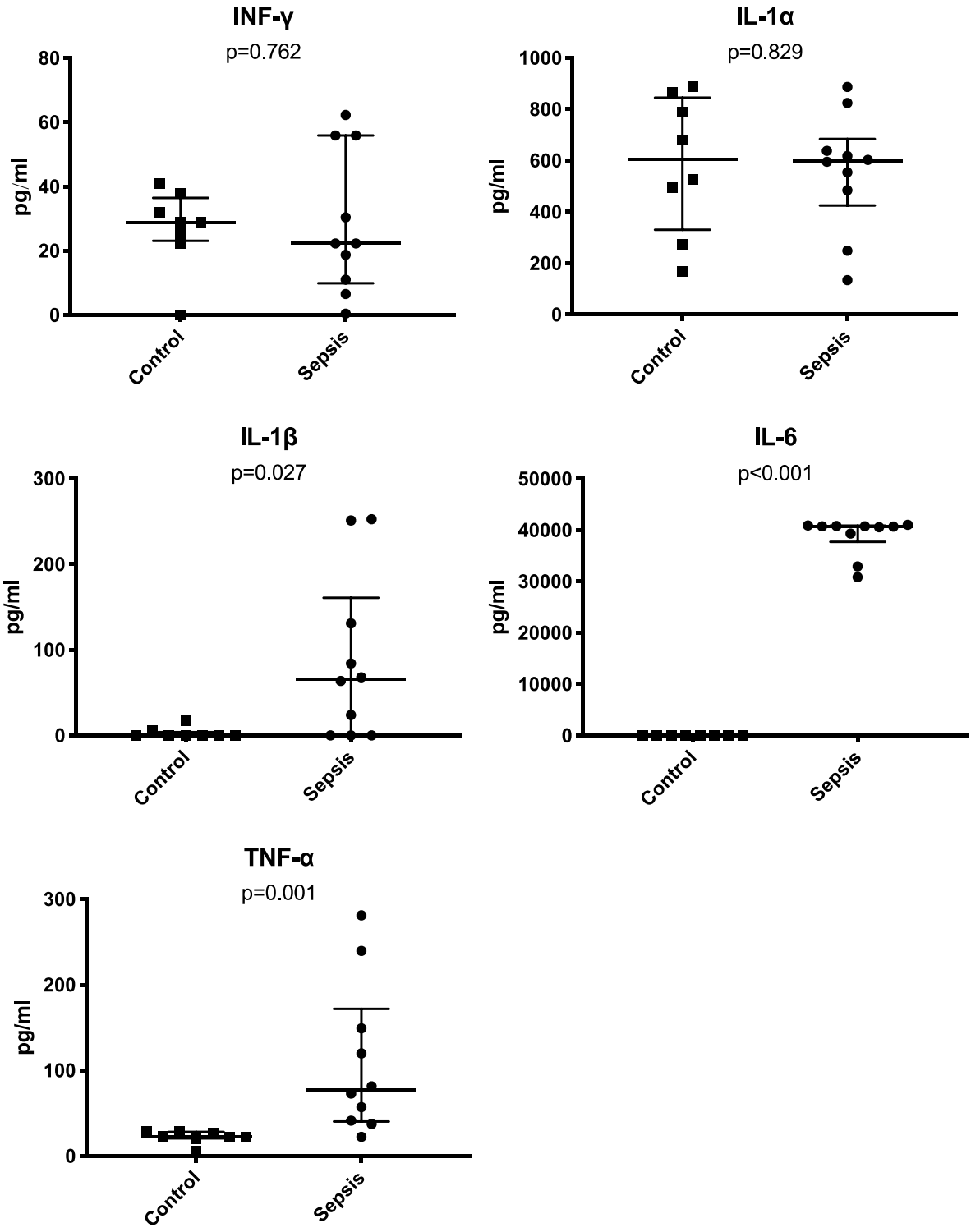

Figure 13: Serum levels of inflammatory cytokines in the two groups. Wide lines represent the means, whiskers the interquartile ranges (IQR). Control group n=8; sepsis group n=10. Statistical comparison: Mann-Whitney-U-Test. This figure is reproduced from (97) (license: http://creativecommons.org/licenses/by/4.0) with permission of the authors.

Functional Permeability Assay (FITC-Dextrane)

Septic animals exhibited significantly increased gut permeability for FITC-Dextrane (FIGURE 14).

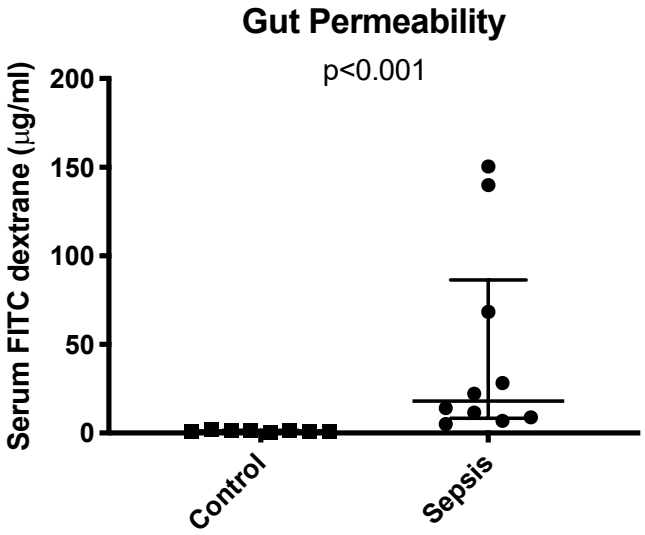

Figure 14: Serum FITC-Dextrane levels. Mann-Whitney-U-Test. Wide line represents the median, whiskers the IQR.

Light Microscopy

Light microscopy identified significant signs of bowel wall inflammation of ileum, jejunum and colon samples in the sepsis group. There were no significant differences for the villus height, crypt depth and the villus height/crypt depth ratio (TABLE 5, TABLE 6 and TABLE 7). No pale cells were found in the Toluidin blue staining in either group.

Table 5: Results of the histological evaluation of ileum samples. Data displayed as median (IQR); MOS...Marsh-Oberhuber Score; CD...crypt depth; VH...villus height. Mann-Whitney-U-Test applied for group comparison.

Item	Control	Sepsis	p-value
MOS	0.1 (0.4)	1.3 (0.8)	**0.003**
CD [µm]	78.1 (12.6)	73.9 (14.9)	0.829
VH [µm]	192.1 (48.7)	188.6 (17.1)	0.696
VH/CD ratio	2.7 (0.3)	2.7 (0.7)	0.965

Table 6: Results of the histological evaluation of colon samples. Data displayed as median (IQR); MOS...Marsh-Oberhuber Score; CD...crypt depth; UH...upfolding height. Mann-Whitney-U-Test applied for group comparison.

Item	Control	Sepsis	p-value
MOS	0.1 (0.4)	1.9 (0.6)	**<0.001**
CD [µm]	56.6 (14.1)	55.4 (10.6)	0.815
UH [µm]	118.7 (19.5)	115.4 (17.8)	0.423
UH/CD ratio	2.2 (1.4)	2.2 (0.3)	0.888

Table 7: Results of the histological evaluation of jejunum samples. Data displayed as median (IQR); MOS...Marsh-Oberhuber Score; CD...crypt depth; VH...villus height;. Mann-Whitney-U-Test applied for group comparison.

Item	Control	Sepsis	p-value
MOS	0.1 (0.7)	1.0 (0.7)	**0.0267**
CD [µm]	74.97 (15.0)	75.98 (21.6)	0.962
VH [µm]	357.2 (89.6)	353.7 (85,2)	0.669
VH/CD ratio	4.7 (1.5)	5.3 (1.5)	0.536

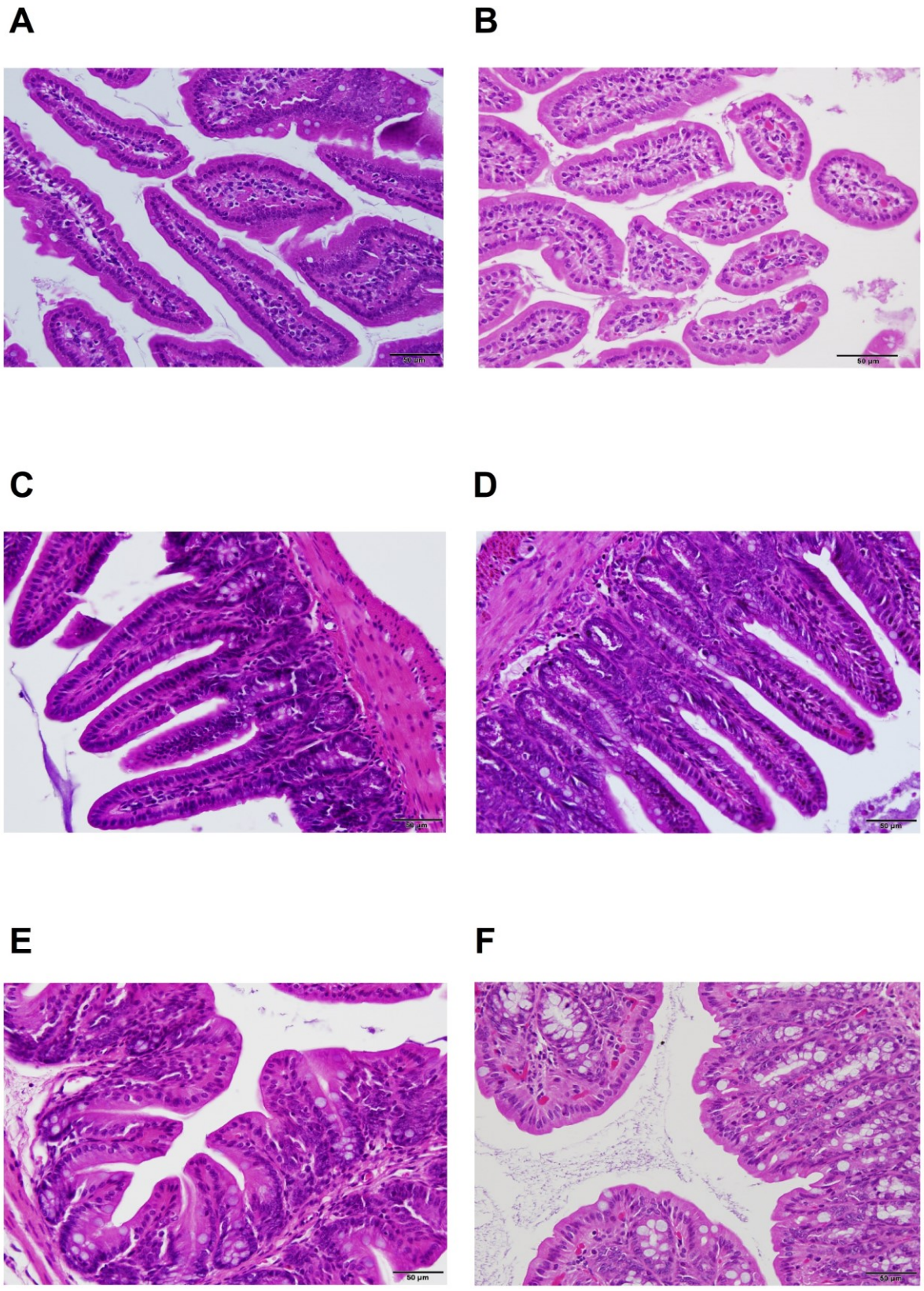

Figure 15: H&E stained examples of bowel wall inflammation in jejunum, ileum and colon of septic and control animals at a magnification of 400 with an oil immersed objective; (A) jejunum control animal,(B) jejunum septic animal, (C) ileum control animal, (D) ileum septic animal, (E) colon control animal, (F) colon septic animal.

Additionally to signs of bowel wall inflammation (FIGURE 15) animals of the septic group also showed a significant widening of the intercellular spaces in the basal region of the IECs in ileum samples (FIGURE 16).

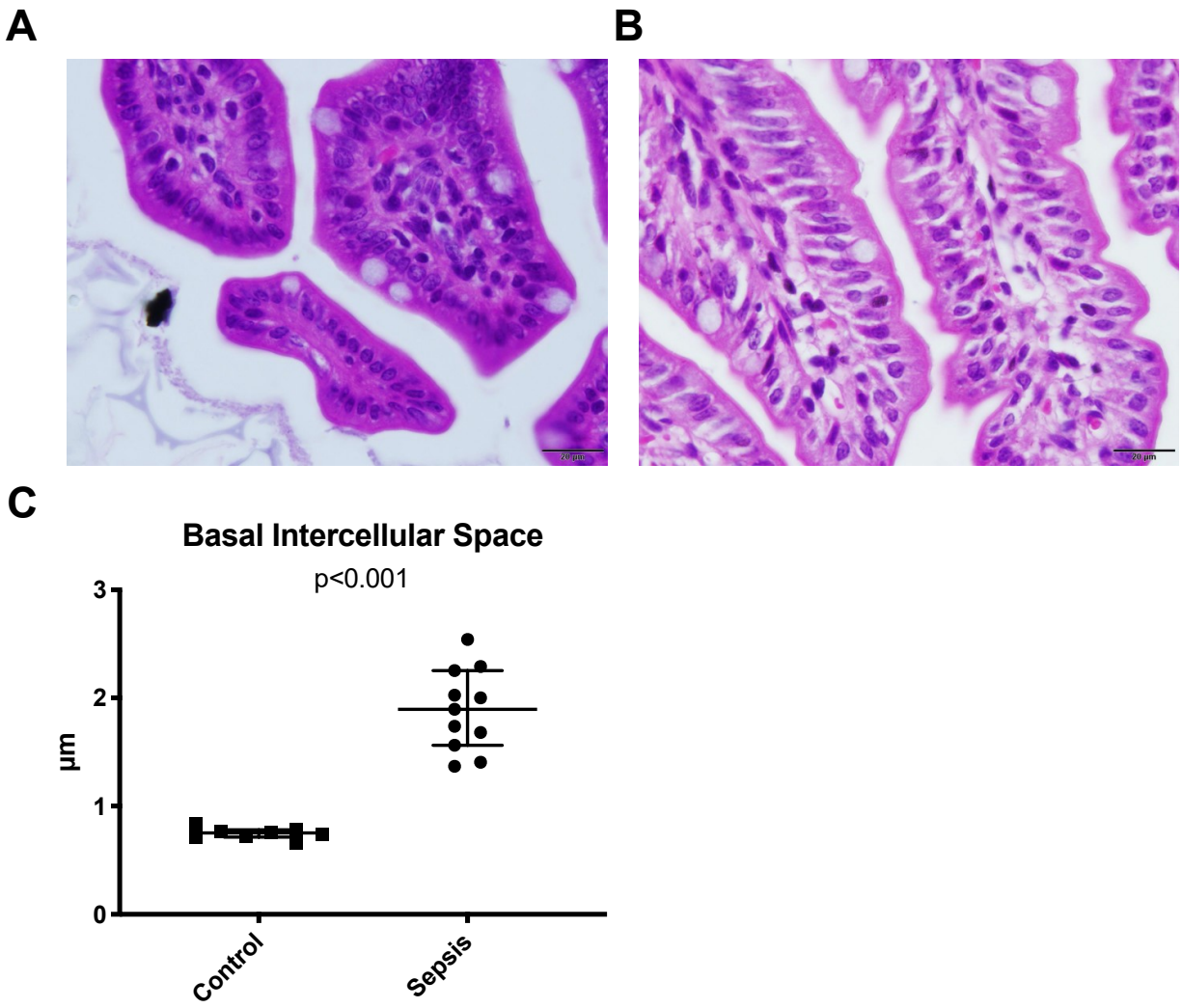

Figure 16: Intercellular space at the basal region of IECs in ileum samples. Panel A: control animal, Panel B: septic animal, Panel C: intercellular distances at the basal layer of IECs. Wide line represents the median, whiskers the IQR. Mann-Whitney-U-Test. The panels A, B and C were extracted from figure 2 (panels H, I and J) of the original publication (97) (license: http://creativecommons.org/licenses/by/4.0) with permission of the authors.

Surface Analysis with Scanning Electron Microscopy (SEM)

SEM did not show any obvious optical differences in ileum or colon samples of the two groups. The surface roughness R_a did not reveal any statistically significant differences between septic and control mice (FIGURE 17).

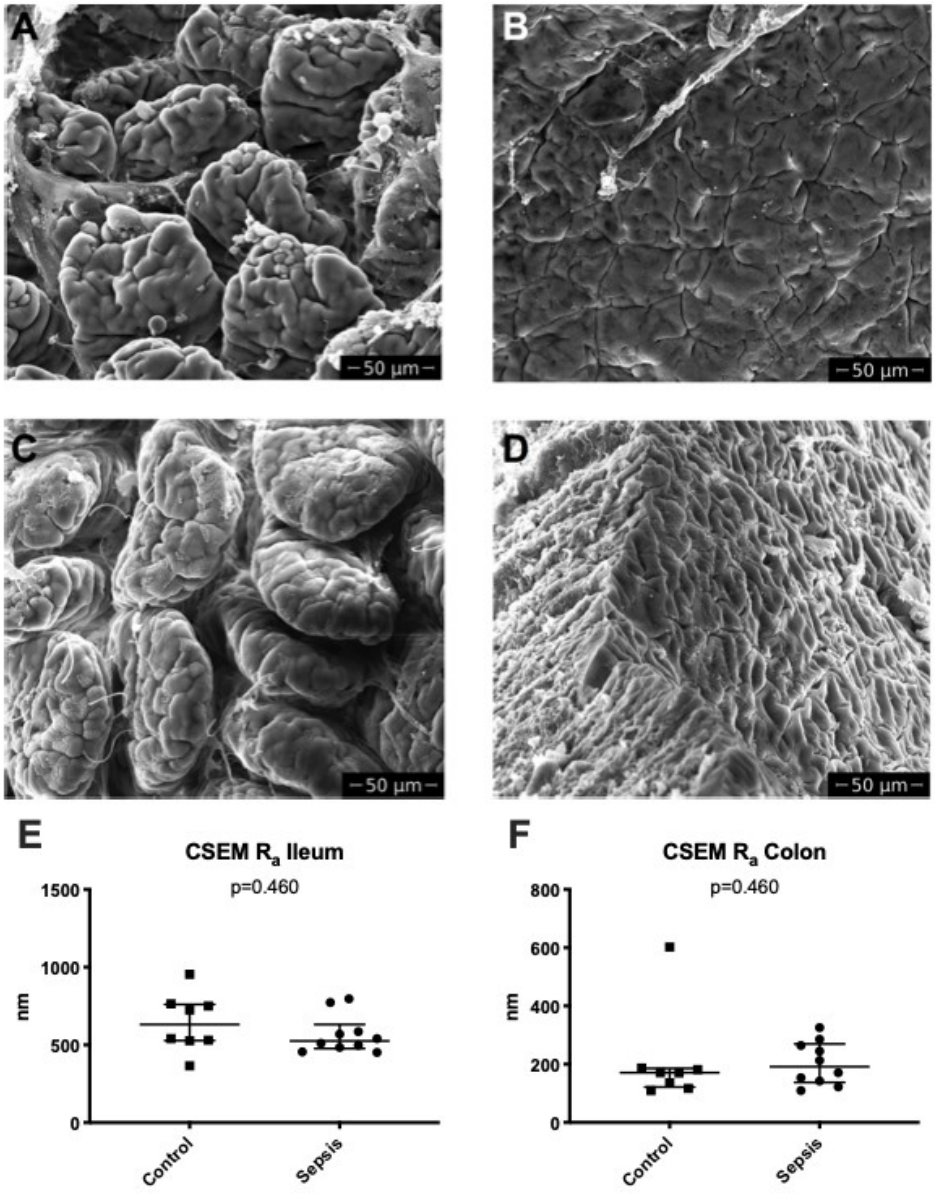

Figure 17: Results and images of SEM analysis. Panel A ileum and B colon of a septic animal; Panel C ileum and D colon of a control animal. The wide lines in the charts in Panels E and F represent the medians, whiskers the IQR. Mann-Whitney-U-Test. Panels A and C were retrieved from figure 2 (panels C and D) of the original publication (97) (http://creativecommons.org/licenses/by/4.0) with permission of the authors.

Transmission Electron Microscopy (TEM) with Analysis of Intercellular Contacts

TEM Analysis showed no statistically significant difference in the height of microvilli between control and sepsis group (control median 120.5nm (IQR 24.0); sepsis median120.5nm (IQR 20.0); p=0.589). A more detailed examination applying the measurements described in the methods section however revealed significantly increased distances at the level of the TJ and AJ in the sepsis group (TABLE 8).

Table 8: Results of the detailed analysis of intercellular distances. Data displayed as median (IQR); Des...Desmosome; AJ...adherens junction; TJ...tight junction. Mann-Whitney-U-Test.

Item	Control	Sepsis	p-value
Des [µm]	0.033 (0.006)	0.034 (0.016)	0.699
AJ [µm]	0.028 (0.006)	0.048 (0.016)	**0.002**
TJ [µm]	0.015 (0.003)	0.019 (0.018)	**0.041**

These results confirmed the findings observed in the H&E stainings and triggered further investigations of the tight junctions.

Analysis of Tight Junction Components

Tight junction components were analyzed in ileum samples of control (n=8) and sepsis (n=10) animals. The tests commenced with an examination of various TJ components at the RNA level by real time PCR showing significant differences in the expression of TJP-1, OCLN, CLDN 2 and CLDN 4 (FIGURE 18).

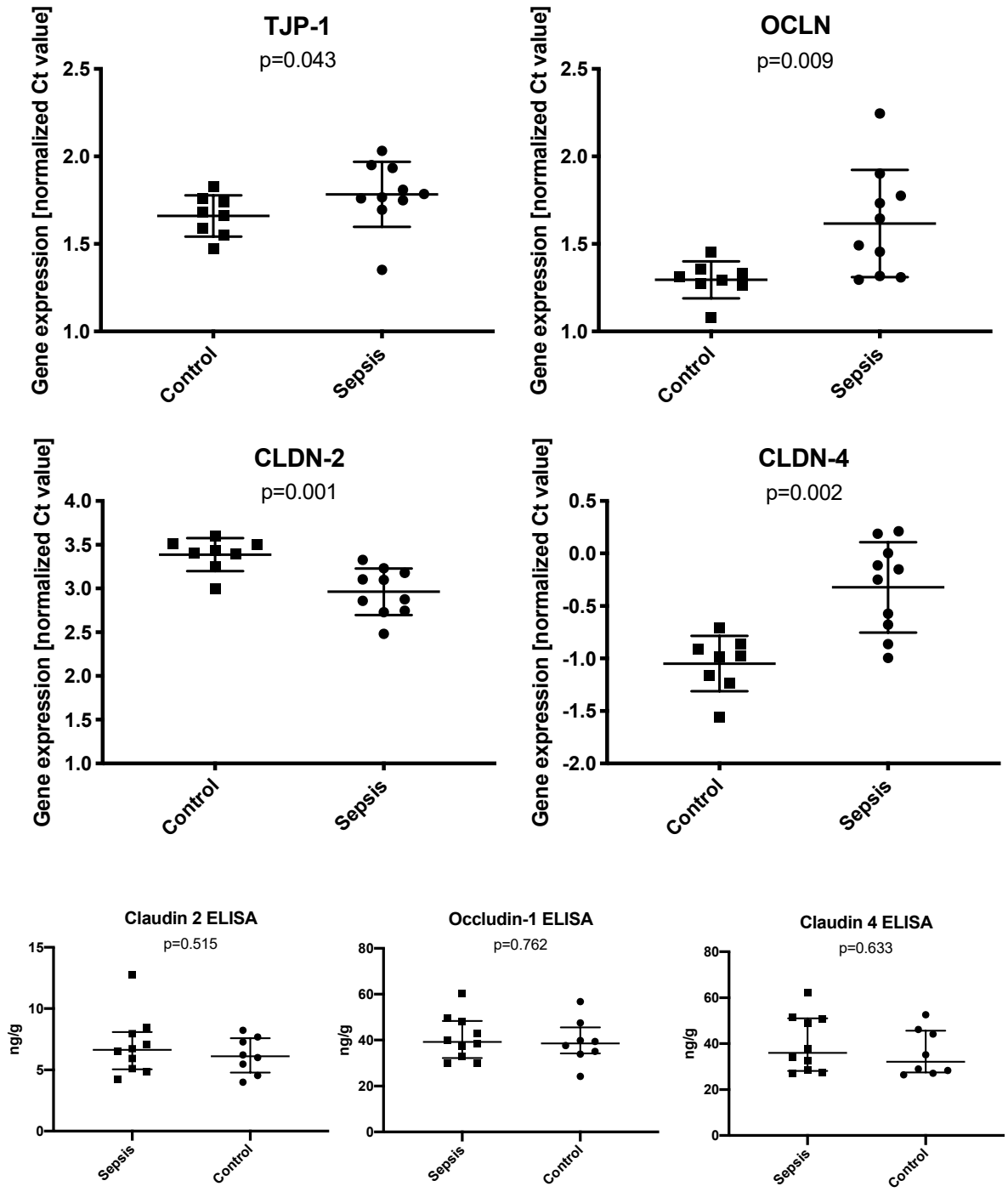

Figure 18: TJ component analysis with PCR and ELISA. The wide lines represent the medians, the whiskers IQR. Mann-Whitney-U-Test. This figure contains graphs (Claudin 2 ELISA, Occludin-1 ELISA and Claudin 4 ELISA) which were reproduced from figure 4 of the original publication (97) (license: http://creativecommons.org/licenses/by/4.0) with permission of the authors.

At the mRNA level TJs of septic animals exhibited an increased expression of CLDN-2 (higher porosity; increased expression is represented in a lower median of normalized Ct values) together with a decreased expression of CLDN-4, OCLN and TJP-1. This phenomenon could not be reproduced at the protein level with ELISA showing no significant differences for the displayed parameters. Expressing the PCR results in fold changes resulted in significant, but low changes for all parameters as possible underlying reason (FIGURE 19).

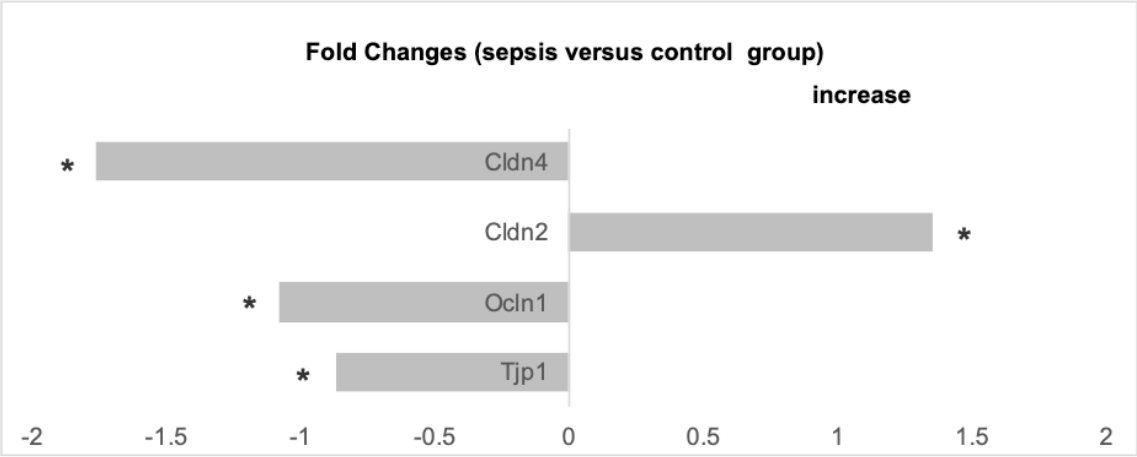

*Figure 19: PCR results normalized for housekeeping genes expressed as fold changes. * marks statistically significant differences (Mann-Whitney-U-Test). This figure was modified (panel A of the original figure was split into two parts) from figure 4 of the original publication (97) (license: http://creativecommons.org/licenses/by/4.0) with permission of the authors.*

Investigations of zonulin as possible regulator of tight junctions by ELISA revealed no statistically significant difference between the two groups (control median 46.1ng/ml (IQR 4.9); sepsis median 47.0ng/ml (IQR 6.9); p=1.0).

IEC Apoptosis

In histological sections of ileum samples, no significant differences could be observed for the rate of apoptotic cells in the group comparison (control median 2.8% (IQR 3.1); sepsis median 1.8% (IQR 3.2); p=0.573). To gain more precise data on IEC apoptosis as possible source for bowel hyper-permeability a PCR analysis for apoptosis marker gene mRNA was conducted. The expression of pro-apoptotic Bax was significantly increased, but the levels of pro-apoptotic Bad and Caspase 3 were significantly decreased in septic animals (FIGURE 20).

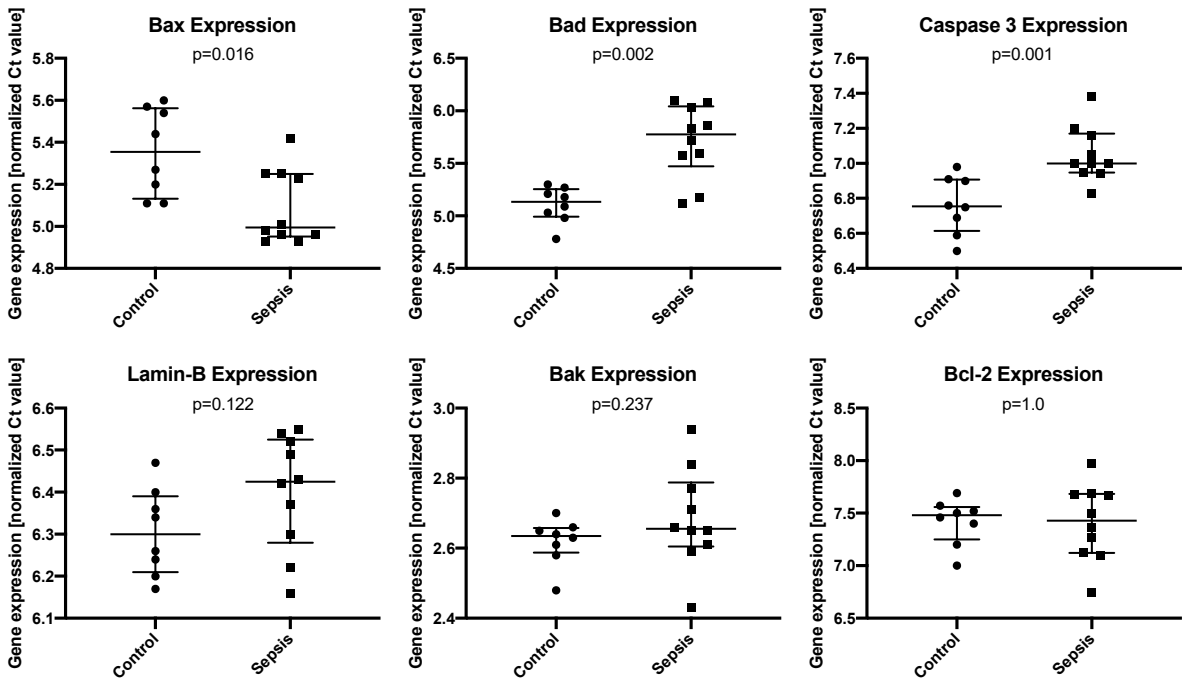

Figure 20: Real time PCR results for apoptosis marker RNA. Wide line represents the median, whiskers the IQR. Mann-Whitney-U-Test.

The expression of the fold-changes of the apoptosis makers (normalized for housekeeping genes) described above reveals low changes between the two groups (FIGURE 21).

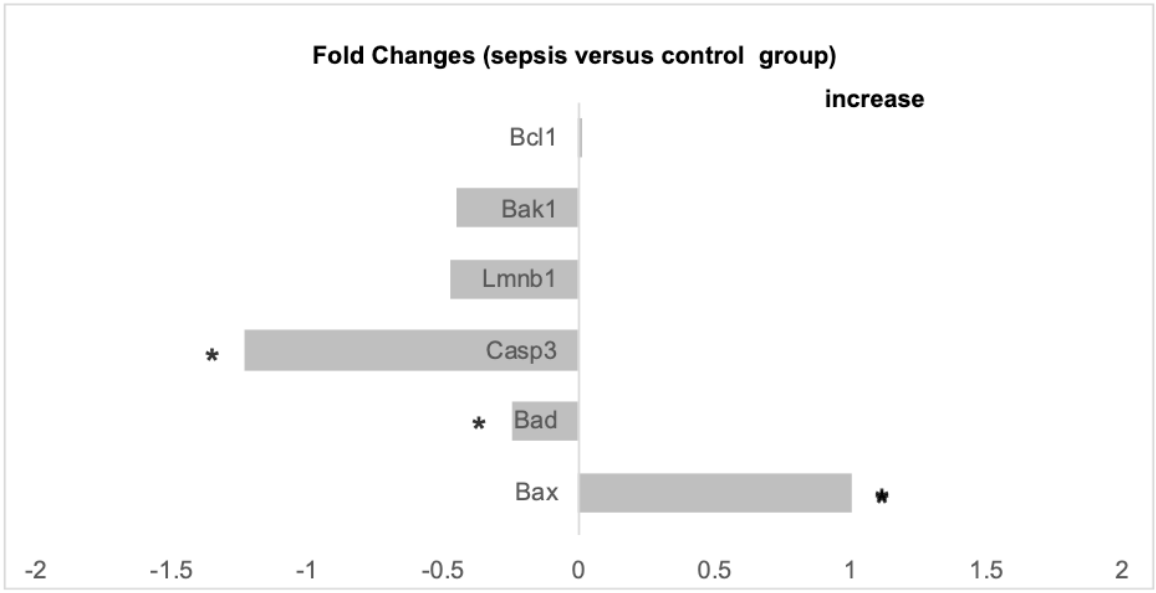

*Figure 21: Fold changes of Apoptosis marker gene PCR. * marks statistically significant differences (Mann-Whitney-U-Test). This figure was modified (Panel A from the original figure was split into two parts) from figure 4 of the original publication (97) (license: http://creativecommons.org/licenses/by/4.0) with the permission of the authors.*

SAXS Analysis of IEC Ultrastructure

Small Angle X-Ray Scattering revealed no obvious optical differences in the curves between the two groups. Similarly, the Porod exponent showed no statistically significant difference of ileum and colon samples between septic and control mice (FIGURE 22).

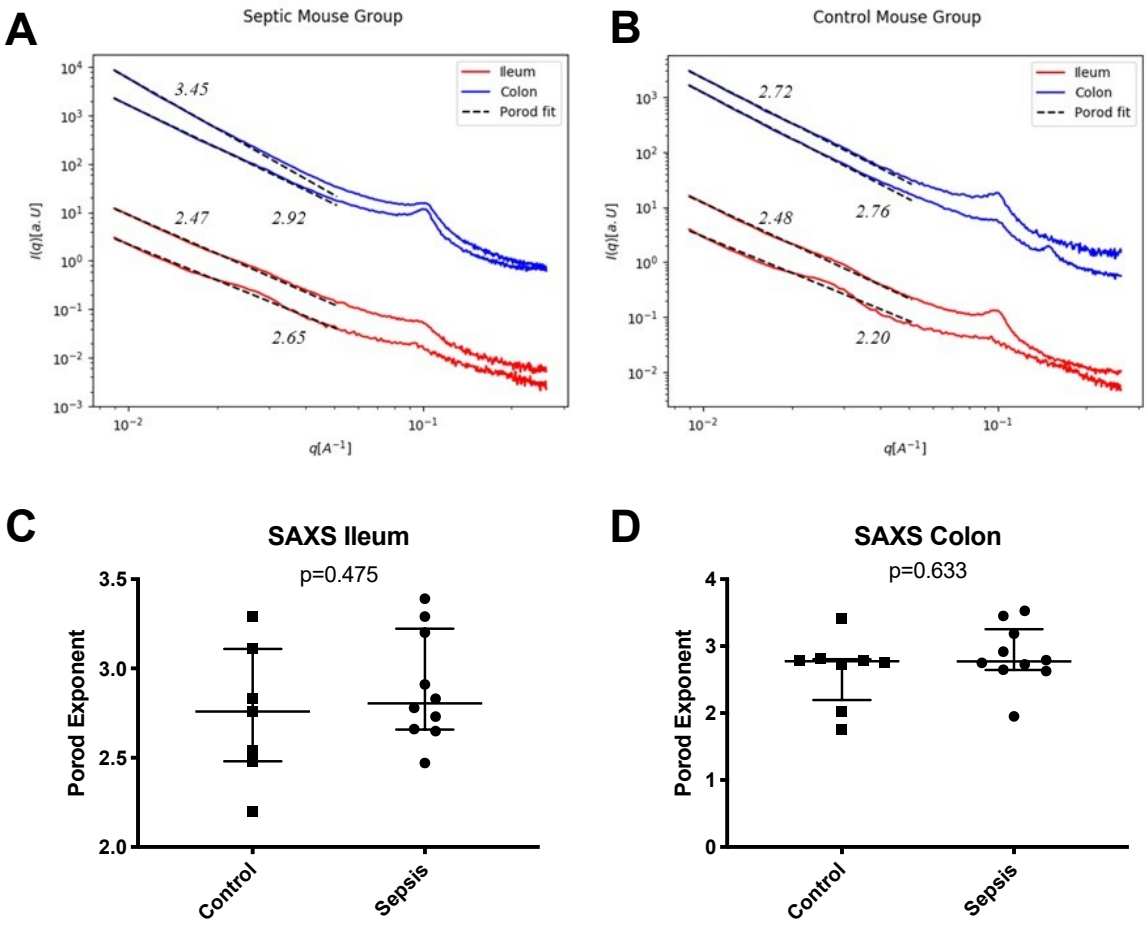

Figure 22: Results of SAXS analysis. Panels A ileum (red) and colon (blue) curves of a septic mouse; Panel B: same parameters for a control animal. Panels C and D Porod exponents. Wide line represents the median, whiskers the IQR. Mann-Whitney-U-Test. This figure is reproduced from (97) (license: http://creativecommons.org/licenses/by/4.0) with permission of the authors.

Correlation Analysis

Correlation analysis showed a statistically significant correlation between FITC-Dextrane levels and the cytokines IL-6 (coefficient 0.520; p=0.027) and TNF-α (coefficient 0.635; p=0.005), as well as the gene expression of OCLN-1 (coefficient 0.649; p=0.004), the intercellular distance at the TJ level (coefficient 0.679; p=0.015) but not with R_a or the Porod exponent.

Discussion

The present study investigated the influence of CLP-induced sepsis on different parameters characterizing the integrity of bowel wall of ileum, jejunum and colon. The major findings were an increased bowel wall permeability for FITC-Dextrane (molecular weight 4kDa, diameter 14 Angstrom) associated with moderate increased gene expression of claudin-2, a reduced gene expression of claudin-4, occludin and tight junction protein 1 as well as widened intercellular spaces at the TJ and AJ level in light and electron microscopy.

Sepsis Model

Cecal ligation and puncture (CLP) has been described as gold standard model for sepsis research (98). This approach has been used by many studies prior to this investigation and can be considered as well-established method (57, 59, 99, 100). Although a common model, there are different ways of achieving CLP: while some authors use single punctures with a 21 G needle (57, 99), others use a 23 G needle and multiple punctures (100). Consequently, the studies also differ in the time points chosen for measurements, endpoints and in the survival rate. Additionally, the authors use different animal models including C57BL/6, BALB/c or other mouse models, in some cases with knock-outs of different genes. These discrepancies in the different approaches to CLP induced sepsis makes a direct comparison difficult. In our setting we chose a model puncturing the cecum 3 times with a 20 G needle, inducing early and severe sepsis. The model has been successfully applied previously by members of the current study group (94). The successful establishment of a septic condition was

observed by increased sepsis scores in the septic group compared to sham operated animals (compare SUPPLEMENT 1).

Systemic Inflammation

As expected septic animals exhibited significantly increased systemic pro-inflammatory cytokine levels. In this regard, IL-1β, IL-6 and TNF-α were increased eight hours after CLP confirming systemic inflammation.

Functional Permeability with FITC-Dextrane

Similar to many other reports in the literature this study revealed an increased intestinal permeability for FITC-Dextrane (57, 60, 61, 101). Different authors have used serum for photometric FITC analysis at very different time points after induction of sepsis. Although this makes comparison of FITC levels difficult, all of them agree on increased FITC-Dextrane serum levels in septic animals. The time points between FITC-Dextrane gavage, CLP and euthanasia in this model were chosen according to other reports in the literature aiming to investigate the early phase of sepsis (100). As described in the introduction, intestinal hyper-permeability can result from different pathologies: epithelial apoptosis, alterations of tight junction composition (100, 102) or status (31, 61) and alterations of the nano-architecture of the bowel wall. This arises the question, which of these factors is associated with increased passage of FITC-Dextrane. While some authors attribute altered TJ composition in septic mice (99, 100) in association with increased serum FITC levels others describe increased IEC apoptosis (101). FITC-Dextrane is available with different molecular weights, which are chosen in accordance with the question to be answered by the study. In the literature

most authors have (similar to us) administered FITC-Dextrane 4SD with a molecular weight of 4kDa in their sepsis models (57, 61, 99, 101). In this regard, it is important to consider the size of FITC-Dextrane 4SD, which is listed with 14 Angstrom (for instance by Sigma Aldrich). There are different possibilities for increased IEC permeability: IEC apoptosis/necrosis, trans-cellular passage or para-cellular passage. The para-cellular pathway again has the options pore pathway (by implementation of different types of claudines) or leak pathway (by changing the status of the tight junction) (28, 44, 45). As already described in the introduction the pore pathway is limited to molecules with a size < 4 Angstrom (28). Larger substances can only pass by means of one of the other IEC alterations. While sepsis may be associated with intestinal hyper-permeability resulting of various different pathways (or a combination of them) it is functionally impossible that increased serum FITC levels are caused by alterations of the TJ protein composition (implementation of different types of claudins). In this investigation this knowledge triggered the search for other mechanisms responsible for FITC hyper-permeability in early sepsis.

Conventional Histology: Bowel Wall and Luminal Surface

In conventional H&E staining septic animals showed marked bowel wall inflammation in jejunum, ileum and colon samples characterized by significantly increased Marsh Oberhuber Scores. In detail, the histological examination confirmed a neutrophil invasion of the bowel wall in septic animals (unpublished observations). This confirms previous reports in the literature describing bowel wall inflammation in ileum (61) and colon (59) samples of septic mice. Hypothetically, this invasion may be associated with increased local levels of inflammatory cytokines. As described above

these factors are triggers for increased permeability of the gut barrier. Therefore, the local inflammation may further fuel hyper-permeability during sepsis.

In their models Dominguez et al. and Perrone et al. have described a significantly reduced villus height and crypt depth in ileum and colon samples of septic mice (99, 101). These findings are in contrast with our data without significant difference of these parameters as well as the crypt depth/villus height ratio. This data is further supported by the SEM analysis of the bowel surface. Optically we could not determine any obvious differences in the SEM images of ileum or colon samples between septic and control mice. A 3D reconstruction of the surface, however, allowed the determination of the surface roughness as objective parameter. Similar to missing discrepancies in light microscopy there were no differences in Ra between septic and control animals. The different approaches to CLP and the different time points of sampling of the different studies can be speculated as the most likely reasons for these discrepancies.

Finally, histological evaluations of the ileum in this study could demonstrate increased intercellular spaces – especially at the basal layers of IECs as possible sign for disruptions of the junctional complex in septic animals. To the best of our knowledge this parameter has hitherto not been published as possible sign for intestinal hyper-permeability.

Evaluation of Tight Junctions

Light microscopy already gave a hint towards increased para-cellular spaces. At the first glance, there seemed to be no obvious changes in TEM of the junctional complex. At closer examination, however, a decrease of electron dense material at the level of the TJ could be observed. This phenomenon has already been published as

sign for disrupted/open tight junctions in ileum and colon samples of septic mice (59, 61). To gain more information, the intercellular distances at the level of TJ, AJ and desmosomes were evaluated in this study. A significantly increased distance at the level of TJ and AJ could be shown in septic animals. The levels of MLCK as most likely regulator for acto-myosin contraction and subsequent opening of TJs were not determined in this investigation but Lorenz et al. demonstrated in a murine knock out model for MLCK that this knock out is associated with an improvement in survival because of a normalization of intestinal gut permeability after CLP induced sepsis (103). Nevertheless, the decrease of electron dense material paired with the increased intercellular distances in TEM (but also in light microscopy) can be interpreted as sign for open/disrupted TJs and increased para-cellular permeability along the leak pathway.

In addition to the leak pathway this study also focused on the pore pathway as possible mechanism for increased para-cellular permeability caused by alterations of tight junction protein composition resulting in increased TJ porosity (99, 100). At the gene level this study revealed significantly increased levels of claudin 2 mRNA together with significantly decreased gene expression levels of claudin-4, TJP-1 and occludin. The increase of claudin 2 paired with a decrease of claudin 4 (among other claudins such as 1, 3, 5, 7 and 8) has been associated with increased TJ porosity and is triggered by cytokine mediated NFkB gene regulation (26, 39, 59, 60). Similar to the results of this investigation other authors also demonstrated modifications of the TJ composition during sepsis (59-61, 99). In detail, Dominguez et al. describe increased claudin 2, without alterations of OCLN or zonulin-1 (ZO-1) in septic mice (99). Yoseph et al. also found increased claudin 2, but also described decreased claudin 5 and OCLN in the jejunum during sepsis (60). In a timeline analysis they could show alterations of claudin 2 as early as 1 hour after CLP. The remaining parameters were

changed 5h after the induction of sepsis (60). Li et al. examined colon samples of septic mice and described an intense staining of claudin 2 together with disruptions of claudins 4 and 5 compared to sham operated animals (59). Hence, most authors agree on increased expressions of claudin 2 during sepsis as also observed in our animals. The discrepancies regarding other TJ components may be attributed to the fact that alterations of the gut barrier are model specific (60). Regarding the results of the PCR in this study it has to be stated that the differences between the groups were significant, but had low biological relevance (due to low fold-changes). An ELISA of ileum samples could not verify the differences observed at the mRNA level. The technique with relatively short incubation times and many samples could have led to different reaction times at different positions on the 96 well plate. Hence, the ELISA results of this study have to be interpreted cautiously. Future studies warrant a different method (for instance Western Blot) or modified protocol for ELISA to gain more representative results on the protein level.

Regarding functional hyper-permeability the significant increase of FITC-Dextrane in the serum of septic mice can only result from leakage and not from altered pore sizes (due to the diameter of FITC-Dextrane 4SD).

Apoptosis of Intestinal Epithelial Cells

Additionally to altered trans- and para-cellular transport a disruption of IECs due to apoptosis may cause intestinal hyper-permeability. Perrone et al. have studied the effect of methicillin resistant *E. coli* on the bowel wall (101). They applied H&E staining, immune-histology for caspase 3 and a western blot for Bax, Bad, Bcl and other apoptosis markers. In their model, they could show an increase of IEC apoptosis in IEC apoptosis in histology. In the Western blot they found an increase of pro-apoptotic

Bax and Bad as well as an increase of anti-apoptotic Bcl-X_L (101) in infected animals (104-108). Similarly, Dominguez et al. and Li et al. could show increased apoptosis of epithelial cells in septic animals (59, 99).

In contrast, our study revealed no increased rate of IEC apoptosis by HOECHST staining of ileum samples in early sepsis. As immune-histology is observer dependent and semi-quantitative we aimed to verify these results with a more objective method. The PCR of the ileum revealed significant, but inconclusive results. The expression of pro-apoptotic Bax was significantly increased in septic animals. At the same time, the expression of pro-apoptotic Bad and Caspase 3 was significantly decreased in these animals. However, the corrected Ct values showed fold changes below 1.5 for all genes investigated questioning the biological relevance of these findings. The relatively shorter time interval between CLP and euthanasia in our experiment as compared to other reports seems to be the most likely reason for the low apoptosis rate.

SAXS and Cellular Ultrastructure

Alterations of the cellular ultrastructure may represent a further reason for intestinal hyper-permeability associated with sepsis. However, data concerning ultrastructural analysis of bowel samples in sepsis are lacking in the literature. There is only a small number of studies applying small-angle X-ray scattering (SAXS) for ultrastructural analysis of organic tissues. Past experiments performed in soft tissue have mainly focused on breast tissue (92, 93, 109). SAXS, however, has not yet been used to experimentally assess the ultrastructure of the bowel wall during sepsis. In the present study we were not able to find alterations of the cellular ultrastructure between control and septic animals as assessed by SAXS. Unlike microscopy techniques,

where local and unique features are depicted, SAXS yields averaged nano-structural parameters of the sample volume irradiated by the beam. Therefore, it is particularly useful for investigating nano-structural features that occur in the irradiated volume in great quantity, because each nanoscale object in the beam contributes to yield an overall detectable scattering signal. Furthermore, the strength of the method lies in the non-destructive nature and the possibility to use it on hydrated soft tissue. In the case of hyper-permeable bowels associated with sepsis, a great amount of nano-sized pores of defined size should yield a distinct shoulder in the SAXS curves in the q range between 0.01 and 0.05A^{-1}. This was, however, not visible in our results. Alternatively, a large distribution of pore sizes could make the shoulder vanish (signal smearing out), but should still be visible in a change of fractal dimension as determined from power law fitting. We therefore suggest that the intestinal hyper-permeability in the early phase of sepsis is not associated with the formation of great numbers and high density of nano-sized pores.

Study Limitations

Limitations of the present study include that we have only assessed the early phase of sepsis 8 hours following CLP. Nevertheless, previous studies have shown that while intestinal permeability is elevated 6 to 48 hours after the onset of sepsis it reaches a peak between 6 and 12 hours following induction of sepsis (100). Moreover, we cannot rule out regional heterogeneity of the different bowel sections regarding the parameters assessed at microscopy.

Conclusion

In conclusion, the present study highlights that bowel wall hyper-permeability in the early phase of experimental polymicrobial sepsis is most likely caused by alterations of the intercellular contacts (AJ and TJ) and not by apoptosis or increases in size or number of nano-pores of intestinal epithelial cells. At the TJ level both increased porosity due to alterations in the TJ protein composition and an opening/disruption of TJs could be observed as causes for intestinal hyper-permeability. Due to its molecular size increased serum FITC-Dextrane levels could only be related to TJ disruptions in this model of early sepsis.

List of Figures

List of Tables

References

1. Gul F, Arslantas MK, Cinel I, Kumar A. Changing Definitions of Sepsis. Turk J Anaesthesiol Reanim. 2017;45(3):129-38.

2. Singer M, Deutschman CS, Seymour CW, Shankar-Hari M, Annane D, Bauer M, et al. The Third International Consensus Definitions for Sepsis and Septic Shock (Sepsis-3). JAMA. 2016;315(8):801-10.

3. Dellinger RP, Levy MM, Rhodes A, Annane D, Gerlach H, Opal SM, et al. Surviving Sepsis Campaign: international guidelines for management of severe sepsis and septic shock, 2012. Intensive Care Med. 2013;39(2):165-228.

4. Vincent JL, Moreno R, Takala J, Willatts S, De Mendonca A, Bruining H, et al. The SOFA (Sepsis-related Organ Failure Assessment) score to describe organ dysfunction/failure. On behalf of the Working Group on Sepsis-Related Problems of the European Society of Intensive Care Medicine. Intensive Care Med. 1996;22(7):707-10.

5. SepNet Critical Care Trials G. Incidence of severe sepsis and septic shock in German intensive care units: the prospective, multicentre INSEP study. Intensive Care Med. 2016;42(12):1980-9.

6. Murphy SL, Kochanek KD, Xu J, Heron M. Deaths: Final Data for 2012. Natl Vital Stat Rep. 2015;63(9):1-117.

7. Melamed A, Sorvillo FJ. The burden of sepsis-associated mortality in the United States from 1999 to 2005: an analysis of multiple-cause-of-death data. Crit Care. 2009;13(1):R28.

8. Dombrovskiy VY, Martin AA, Sunderram J, Paz HL. Rapid increase in hospitalization and mortality rates for severe sepsis in the United States: a trend analysis from 1993 to 2003. Crit Care Med. 2007;35(5):1244-50.

9. Vachharajani V. Influence of obesity on sepsis. Pathophysiology. 2008;15(2):123-34.

10. Cavaillon JM. Pro- versus anti-inflammatory cytokines: myth or reality. Cell Mol Biol (Noisy-le-grand). 2001;47(4):695-702.

11. Schulte W, Bernhagen J, Bucala R. Cytokines in sepsis: potent immunoregulators and potential therapeutic targets--an updated view. Mediators Inflamm. 2013;2013:165974.

12. Hoyt DB. Looking forward. The Trauma, Critical Care and Acute Care Surgery program. Bull Am Coll Surg. 2012;97(2):4-5.

13. Prin M, Bakker J, Wagener G. Hepatosplanchnic circulation in cirrhosis and sepsis. World J Gastroenterol. 2015;21(9):2582-92.

14. Deitch EA. Bacterial translocation or lymphatic drainage of toxic products from the gut: what is important in human beings? Surgery. 2002;131(3):241-4.

15. Cepinskas G, Wilson JX. Inflammatory response in microvascular endothelium in sepsis: role of oxidants. J Clin Biochem Nutr. 2008;42(3):175-84.

16. Morelli A, Passariello M. Hemodynamic coherence in sepsis. Best Pract Res Clin Anaesthesiol. 2016;30(4):453-63.

17. De Backer D, Creteur J, Preiser JC, Dubois MJ, Vincent JL. Microvascular blood flow is altered in patients with sepsis. Am J Respir Crit Care Med. 2002;166(1):98-104.

18. Podolsky DK. Mucosal immunity and inflammation. V. Innate mechanisms of mucosal defense and repair: the best offense is a good defense. Am J Physiol. 1999;277(3):G495-9.

19. Helander HF, Fandriks L. Surface area of the digestive tract - revisited. Scand J Gastroenterol. 2014;49(6):681-9.

20. Radeva MY, Waschke J. Mind the gap: mechanisms regulating the endothelial barrier. Acta Physiol (Oxf). 2018;222(1).

21. Clevers HC, Bevins CL. Paneth cells: maestros of the small intestinal crypts. Annu Rev Physiol. 2013;75:289-311.

22. Elphick DA, Mahida YR. Paneth cells: their role in innate immunity and inflammatory disease. Gut. 2005;54(12):1802-9.

23. Gelberg HB. Comparative anatomy, physiology, and mechanisms of disease production of the esophagus, stomach, and small intestine. Toxicol Pathol. 2014;42(1):54-66.

24. Franke WW. Discovering the molecular components of intercellular junctions--a historical view. Cold Spring Harb Perspect Biol. 2009;1(3):a003061.

25. Stadnyk AW. Intestinal epithelial cells as a source of inflammatory cytokines and chemokines. Can J Gastroenterol. 2002;16(4):241-6.

26. Gunzel D, Yu AS. Claudins and the modulation of tight junction permeability. Physiol Rev. 2013;93(2):525-69.

27. Piton G, Capellier G. Biomarkers of gut barrier failure in the ICU. Curr Opin Crit Care. 2016;22(2):152-60.

28. Rainer F. Morphologic Alterations of Small Intestinal Mucosa in Patients with Cirrhosis. Graz, AUSTRIA: Medical University of Graz, Austria; 2013.

29. Bauer HC, Traweger A, Zweimueller-Mayer J, Lehner C, Tempfer H, Krizbai I, et al. New aspects of the molecular constituents of tissue barriers. J Neural Transm (Vienna). 2011;118(1):7-21.

30. Will C, Fromm M, Muller D. Claudin tight junction proteins: novel aspects in paracellular transport. Perit Dial Int. 2008;28(6):577-84.

31. Li Q, Zhang Q, Zhang M, Wang C, Zhu Z, Li N, et al. Effect of n-3 polyunsaturated fatty acids on membrane microdomain localization of tight junction proteins in experimental colitis. FEBS J. 2008;275(3):411-20.

32. Krause G, Winkler L, Mueller SL, Haseloff RF, Piontek J, Blasig IE. Structure and function of claudins. Biochim Biophys Acta. 2008;1778(3):631-45.

33. Ermund A, Schutte A, Johansson ME, Gustafsson JK, Hansson GC. Studies of mucus in mouse stomach, small intestine, and colon. I. Gastrointestinal mucus layers have different properties depending on location as well as over the Peyer's patches. Am J Physiol Gastrointest Liver Physiol. 2013;305(5):G341-7.

34. Rodriguez-Pineiro AM, Bergstrom JH, Ermund A, Gustafsson JK, Schutte A, Johansson ME, et al. Studies of mucus in mouse stomach, small intestine, and colon. II. Gastrointestinal mucus proteome reveals Muc2 and Muc5ac accompanied by a set of core proteins. Am J Physiol Gastrointest Liver Physiol. 2013;305(5):G348-56.

35. Johansson ME, Larsson JM, Hansson GC. The two mucus layers of colon are organized by the MUC2 mucin, whereas the outer layer is a legislator of host-microbial interactions. Proc Natl Acad Sci U S A. 2011;108 Suppl 1:4659-65.

36. Kim YS, Ho SB. Intestinal goblet cells and mucins in health and disease: recent insights and progress. Curr Gastroenterol Rep. 2010;12(5):319-30.

37. Schneider H, Pelaseyed T, Svensson F, Johansson MEV. Study of mucin turnover in the small intestine by in vivo labeling. Sci Rep. 2018;8(1):5760.

38. Dharmani P, Srivastava V, Kissoon-Singh V, Chadee K. Role of intestinal mucins in innate host defense mechanisms against pathogens. J Innate Immun. 2009;1(2):123-35.

39. Haussner F, Chakraborty S, Halbgebauer R, Huber-Lang M. Challenge to the Intestinal Mucosa During Sepsis. Front Immunol. 2019;10:891.

40. Kierzenbaum A, Tres L. Histology and Cell Biology: An Introduction to Pathology. 5 ed. St. Louis: Mosby; 2002.

41. Levine DS, Haggitt RC. Normal histology of the colon. Am J Surg Pathol. 1989;13(11):966-84.

42. Madara JL. Warner-Lambert/Parke-Davis Award lecture. Pathobiology of the intestinal epithelial barrier. Am J Pathol. 1990;137(6):1273-81.

43. Anderson JM. Molecular structure of tight junctions and their role in epithelial transport. News Physiol Sci. 2001;16:126-30.

44. Anderson JM, Van Itallie CM. Physiology and function of the tight junction. Cold Spring Harb Perspect Biol. 2009;1(2):a002584.

45. Citi S, Cordenonsi M. Tight junction proteins. Biochim Biophys Acta. 1998;1448(1):1-11.

46. Al-Sadi R, Guo S, Dokladny K, Smith MA, Ye D, Kaza A, et al. Mechanism of interleukin-1beta induced-increase in mouse intestinal permeability in vivo. J Interferon Cytokine Res. 2012;32(10):474-84.

47. Al-Sadi R, Ye D, Said HM, Ma TY. Cellular and molecular mechanism of interleukin-1beta modulation of Caco-2 intestinal epithelial tight junction barrier. J Cell Mol Med. 2011;15(4):970-82.

48. Colgan SP, Resnick MB, Parkos CA, Delp-Archer C, McGuirk D, Bacarra AE, et al. IL-4 directly modulates function of a model human intestinal epithelium. J Immunol. 1994;153(5):2122-9.

49. Yang R, Han X, Uchiyama T, Watkins SK, Yaguchi A, Delude RL, et al. IL-6 is essential for development of gut barrier dysfunction after hemorrhagic shock and resuscitation in mice. Am J Physiol Gastrointest Liver Physiol. 2003;285(3):G621-9.

50. Costantini TW, Deree J, Loomis W, Putnam JG, Choi S, Baird A, et al. Phosphodiesterase inhibition attenuates alterations to the tight junction proteins occludin and ZO-1 in immunostimulated Caco-2 intestinal monolayers. Life Sci. 2009;84(1-2):18-22.

51. Yajima S, Morisaki H, Serita R, Suzuki T, Katori N, Asahara T, et al. Tumor necrosis factor-alpha mediates hyperglycemia-augmented gut barrier dysfunction in endotoxemia. Crit Care Med. 2009;37(3):1024-30.

52. Beaurepaire C, Smyth D, McKay DM. Interferon-gamma regulation of intestinal epithelial permeability. J Interferon Cytokine Res. 2009;29(3):133-44.

53. Luyer MD, Buurman WA, Hadfoune M, Wolfs T, van't Veer C, Jacobs JA, et al. Exposure to bacterial DNA before hemorrhagic shock strongly aggravates systemic inflammation and gut barrier loss via an IFN-gamma-dependent route. Ann Surg. 2007;245(5):795-802.

54. Upperman JS, Potoka D, Grishin A, Hackam D, Zamora R, Ford HR. Mechanisms of nitric oxide-mediated intestinal barrier failure in necrotizing enterocolitis. Semin Pediatr Surg. 2005;14(3):159-66.

55. Lejeune M, Leung P, Beck PL, Chadee K. Role of EP4 receptor and prostaglandin transporter in prostaglandin E2-induced alteration in colonic epithelial barrier integrity. Am J Physiol Gastrointest Liver Physiol. 2010;299(5):G1097-105.

56. Rodriguez-Lagunas MJ, Ferrer R, Moreno JJ. Effect of eicosapentaenoic acid-derived prostaglandin E3 on intestinal epithelial barrier function. Prostaglandins Leukot Essent Fatty Acids. 2013;88(5):339-45.

57. Short SS, Wang J, Castle SL, Fernandez GE, Smiley N, Zobel M, et al. Low doses of celecoxib attenuate gut barrier failure during experimental peritonitis. Laboratory investigation; a journal of technical methods and pathology. 2013;93(12):1265-75.

58. Puppa MJ, White JP, Sato S, Cairns M, Baynes JW, Carson JA. Gut barrier dysfunction in the Apc(Min/+) mouse model of colon cancer cachexia. Biochim Biophys Acta. 2011;1812(12):1601-6.

59. Li Q, Zhang Q, Wang C, Liu X, Li N, Li J. Disruption of tight junctions during polymicrobial sepsis in vivo. J Pathol. 2009;218(2):210-21.

60. Yoseph BP, Klingensmith NJ, Liang Z, Breed ER, Burd EM, Mittal R, et al. Mechanisms of Intestinal Barrier Dysfunction in Sepsis. Shock. 2016;46(1):52-9.

61. Zhou H, Liang H, Li ZF, Xiang H, Liu W, Li JG. Vagus nerve stimulation attenuates intestinal epithelial tight junctions disruption in endotoxemic mice through alpha7 nicotinic acetylcholine receptors. Shock. 2013;40(2):144-51.

62. Moriez R, Salvador-Cartier C, Theodorou V, Fioramonti J, Eutamene H, Bueno L. Myosin light chain kinase is involved in lipopolysaccharide-induced disruption of colonic epithelial barrier and bacterial translocation in rats. Am J Pathol. 2005;167(4):1071-9.

63. Turner JR. Molecular basis of epithelial barrier regulation: from basic mechanisms to clinical application. Am J Pathol. 2006;169(6):1901-9.

64. Ye D, Ma I, Ma TY. Molecular mechanism of tumor necrosis factor-alpha modulation of intestinal epithelial tight junction barrier. Am J Physiol Gastrointest Liver Physiol. 2006;290(3):G496-504.

65. Hotchkiss RS, Swanson PE, Freeman BD, Tinsley KW, Cobb JP, Matuschak GM, et al. Apoptotic cell death in patients with sepsis, shock, and multiple organ dysfunction. Crit Care Med. 1999;27(7):1230-51.

66. Zhang L, Meng Q, Yepuri N, Wang G, Xi X, Cooney RN. Surfactant Proteins-A and -D Attenuate LPS-Induced Apoptosis in Primary Intestinal Epithelial Cells (IECs). Shock. 2018;49(1):90-8.

67. Zheng D, Yu Y, Li M, Wang G, Chen R, Fan GC, et al. Inhibition of MicroRNA 195 Prevents Apoptosis and Multiple-Organ Injury in Mouse Models of Sepsis. J Infect Dis. 2016;213(10):1661-70.

68. Jiang LY, Zhang M, Zhou TE, Yang ZF, Wen LQ, Chang JX. Changes of the immunological barrier of intestinal mucosa in rats with sepsis. World J Emerg Med. 2010;1(2):138-43.

69. Swank GM, Deitch EA. Role of the gut in multiple organ failure: bacterial translocation and permeability changes. World J Surg. 1996;20(4):411-7.

70. Qin X, Caputo FJ, Xu DZ, Deitch EA. Hydrophobicity of mucosal surface and its relationship to gut barrier function. Shock. 2008;29(3):372-6.

71. Lankelma JM, van Vught LA, Belzer C, Schultz MJ, van der Poll T, de Vos WM, et al. Critically ill patients demonstrate large interpersonal variation in intestinal microbiota dysregulation: a pilot study. Intensive Care Med. 2017;43(1):59-68.

72. Kawano M, Miyoshi M, Ogawa A, Sakai F, Kadooka Y. Lactobacillus gasseri SBT2055 inhibits adipose tissue inflammation and intestinal permeability in mice fed a high-fat diet. J Nutr Sci. 2016;5:e23.

73. Tong LC, Wang Y, Wang ZB, Liu WY, Sun S, Li L, et al. Propionate Ameliorates Dextran Sodium Sulfate-Induced Colitis by Improving Intestinal Barrier Function and Reducing Inflammation and Oxidative Stress. Front Pharmacol. 2016;7:253.

74. Gulbins E, Jekle A, Ferlinz K, Grassme H, Lang F. Physiology of apoptosis. Am J Physiol Renal Physiol. 2000;279(4):F605-15.

75. Leong TY, Cooper K, Leong AS. Immunohistology--past, present, and future. Adv Anat Pathol. 2010;17(6):404-18.

76. Leong AS. Quantitation in immunohistology: fact or fiction? A discussion of variables that influence results. Appl Immunohistochem Mol Morphol. 2004;12(1):1-7.

77. Elmore S. Apoptosis: a review of programmed cell death. Toxicol Pathol. 2007;35(4):495-516.

78. Muppidi J, Porter M, Siegel RM. Measurement of apoptosis and other forms of cell death. Curr Protoc Immunol. 2004;Chapter 3:Unit 3 17.

79. Mizuta T, Shimizu S, Matsuoka Y, Nakagawa T, Tsujimoto Y. A Bax/Bak-independent mechanism of cytochrome c release. J Biol Chem. 2007;282(22):16623-30.

80. Rohe I, Huttner FJ, Plendl J, Drewes B, Zentek J. Comparison of different histological protocols for the preservation and quantification of the intestinal mucus layer in pigs. Eur J Histochem. 2018;62(1):2874.

81. Morini G, Grandi D, Arcari ML, Galanti G, Bertaccini G. Histological effect of (R)-alpha-methylhistamine on ethanol damage in rat gastric mucosa: influence on mucus production. Dig Dis Sci. 1997;42(5):1020-8.

82. Fragkos KC, Forbes A. Citrulline as a marker of intestinal function and absorption in clinical settings: A systematic review and meta-analysis. United European Gastroenterol J. 2018;6(2):181-91.

83. Crenn P, Vahedi K, Lavergne-Slove A, Cynober L, Matuchansky C, Messing B. Plasma citrulline: A marker of enterocyte mass in villous atrophy-associated small bowel disease. Gastroenterology. 2003;124(5):1210-9.

84. Guzel A, Kanter M, Guzel A, Yucel AF, Erboga M. Protective effect of curcumin on acute lung injury induced by intestinal ischaemia/reperfusion. Toxicol Ind Health. 2013;29(7):633-42.

85. Matsumoto S, Sekine K, Funaoka H, Yamazaki M, Shimizu M, Hayashida K, et al. Diagnostic performance of plasma biomarkers in patients with acute intestinal ischaemia. Br J Surg. 2014;101(3):232-8.

86. Sui T, Sandholzer M, Lunt A, Baimpas N, Smith A, Landini G, et al. In situ X-ray scattering evaluation of heat-induced uiltrastructural changes in dental tissues and synthetic hydroxyapatite. J R Soc Interface. 2014;11:1-12.

87. Di Cola E, Grillo I, SRistori S. Small Angle X-ray and Neuron Scattering: Powerful Tools for Studying the Structure of Drug Loaded Liposomes. Pharmaceutics. 2016;8(10):1-16.

88. Fratzl P. Statistical model of the habit and arrangement of mineral crystals in the collagen of bone. J Statistical Physics. 1994;77(1-2):125-43.

89. Lichtenegger H, Reiterer A, Stranzl-Tschegg S, Fratzl P. Variation of cellulose microfibril angles in softwoods and hardwoods - a possible strategy of mechanical optimization. J Struct Biol. 1999;128(3):257-69.

90. Pabisch S, AWagermaier W, Zander T, Li C, Fratzl P. Imaging the nanostructure of bone and dentin through small.- and wide-angle X-ray scattering. Methods Enzymol. 2013;532:391-413.

91. Poundarik A, Boskey A, Gunberg C, SVashishth D. Biomolecular regulation, composition and nanoarchitecture of bone mineral. Nature. 2018;1191(8):1-8.

92. Fernández M, Suhonen H, Keyrilainen J, Bravin A, Fiedler S, Karjalainen-Linsberg M, et al. USAXS and SAXS from cnancer-bearing breast tissue samples. Eur J Radiology. 2008;68S:S89-S94.

93. Sidhu S, Falzon G, SA. H, Fox J, Lewis R, KKW. S. Classification of breast tissue using a laboratory system for small-angle x-ray scattering (SAXS). Phys Med Biol. 2011;56:6779-91.

94. Singer G, Urakami H, Specian RD, Stokes KY, Granger DN. Platelet recruitment in the murine hepatic microvasculature during experimental sepsis: role of neutrophils. Microcirculation. 2006;13(2):89-97.

95. Adelman D, Murray J, Wu T, Mäki M, Green P, CP K. Measuring change in small intestinal histology in patients with celiac disease. Am J Gastroenterol. 2018;online first 02/2018.

96. Buchheister S, Buettner M, Basic M, Noack A, Breves G, Buchen B, et al. CD14 Plays a Protective Role in Experimental Inflammatory Bowel Disease by Enhancing Intestinal Barrier Function. Am J Pathol. 2017;187(5):1106-20.

97. Obermuller B, Frisina N, Meischel M, Singer G, Stanzl-Tschegg S, Lichtenegger H, et al. Examination of intestinal ultrastructure, bowel wall apoptosis and tight junctions in the early phase of sepsis. Sci Rep. 2020;10(1):11507.

98. Wichterman KA, Baue AE, Chaudry IH. Sepsis and septic shock--a review of laboratory models and a proposal. J Surg Res. 1980;29(2):189-201.

99. Dominguez J, Samoccha A, Liang Z, Burd E, Farris A, Coopersmith C. Inhibition of IKKb in enterocytes exacerbates sepsis-induced intestinal injury and wordsens mortality. Crit Care Med. 2013;41(10):e275-e85.

100. Yoseph B, Klingensmith N, Liang Z, Breed E, Burd E, Mittal R, et al. Mechanisms of intestinal barrier dysfunction in sepsis. Shock. 2016;46(1):52-9.

101. Perrone EE, Jung E, Breed E, Dominguez JA, Liang Z, Clark AT, et al. Mechanisms of methicillin-resistant Staphylococcus aureus pneumonia-induced intestinal epithelial apoptosis. Shock. 2012;38(1):68-75.

102. Zeissig S, Burgel N, Gunzel D, Richter J, Mankertz J, Wahnschaffe U, et al. Changes in expression and distribution of claudin 2, 5 and 8 lead to discontinuous tight junctions and barrier dysfunction in active Crohn's disease. Gut. 2007;56(1):61-72.

103. Lorentz CA, Liang Z, Meng M, Chen CW, Yoseph BP, Breed ER, et al. Myosin light chain kinase knockout improves gut barrier function and confers a survival advantage in polymicrobial sepsis. Mol Med. 2017;23:155-65.

104. Hotchkiss RS, Swanson PE, Knudson CM, Chang KC, Cobb JP, Osborne DF, et al. Overexpression of Bcl-2 in transgenic mice decreases apoptosis and improves survival in sepsis. J Immunol. 1999;162(7):4148-56.

105. Inoue S, Unsinger J, Davis CG, Muenzer JT, Ferguson TA, Chang K, et al. IL-15 prevents apoptosis, reverses innate and adaptive immune dysfunction, and improves survival in sepsis. J Immunol. 2010;184(3):1401-9.

106. Otani S, Oami T, Yoseph BP, Klingensmith NJ, Chen CW, Liang Z, et al. Overexpression of BCL-2 in the Intestinal Epithelium Prevents Sepsis-Induced Gut Barrier Function Via Altering Tight Junction Protein Expression. Shock. 2019.

107. Stromberg PE, Woolsey CA, Clark AT, Clark JA, Turnbull IR, McConnell KW, et al. CD4+ lymphocytes control gut epithelial apoptosis and mediate survival in sepsis. FASEB J. 2009;23(6):1817-25.

108. Turnbull IR, Buchman TG, Javadi P, Woolsey CA, Hotchkiss RS, Karl IE, et al. Age disproportionately increases sepsis-induced apoptosis in the spleen and gut epithelium. Shock. 2004;22(4):364-8.

109. Conceicao A, Antoniassi M, Poletti M. Analysis of breast cancer by small angle X-ray scattering (SAXS). Analyst. 2009;134(6):1077-82.

Supplement 1: Clinical determination of the sepsis score

Determination of humane endpoint criteria in animal experiments

Observation	Score
I Body weight	
-unaffected or weight gain	0
-alteration < 5%	1
-Weight loss 5-10%	5
-Weight loss 11-20%	10
-Weight loss >20%	20
II General health condition	
-smooth and shiny fur; clean orifices; clear and shiny eyes	0
-change of the fur (reduce or excessive body care)	1
-rough hair coat, unkempt appearance, neglected orifices, abnormal skin surface (small wounds), cloudy eyes, discharge form eyes, starting/minor rectal prolapse, abnormal posture, increased muscle tone	5
-rough and dirty hair coat, humid orifices (stuck together), moderate rectal prolapse, dehydration, abnormal posture, cloudy eyes, excessive muscle tone	10
-cramps, paralysis (trunk muscles, extremities); breath sounds; severe rectal prolapse	20
III Behavior	
-normal behaviour (sleeping, the animal shows a reaction to blowing and touch, curiosity, social interaction)	0
-slight deviations of the normal behaviour	1
-unusual behaviour, limited motor activity or hyperkinetic	5
-isolation, lethargy; excessive hyperkinetic or behavioural stereotypy; disorder of coordination	10
-Pain sounds while seizing; Self-induced trauma (autoaggression)	20
IV Clinical findings	

-normal temperature an respiration, warm extremities, Mucous membranes are well supplied with blood, normal abdomen	0
-slight deviations of the normal situation	1
-the animal feels colder as normal, cold extremities, pale mucous membranes	5
-moderate deviation of the temperature, respiration + or – 30%, enlarged abdomen	10
-high deviations of the temperature, respiration + or – 50%, blood in urine of feces, diameter of a pressable tumour > 2com (in rodents)	20
V Study specific humane endpoints	
OP wound closed, skin around normal	0
OP wound closed, skin around reddish	1
OP wound slightly opened at one point in the upper layer, skin around red	5
OP wound slightly opened at more than one point in the upper layer, skin around red with starting grey boundary of the wound	10
OP wound opened at one point in both layers or completely in the upper layer, skin around red with starting gangrene	20

Evaluation, Measures	**Sum of scores**
Stress level 0= no stress	0
Stress level 1= slight level of stress, note in PyRat, to be observed carefully	1-9
Stress level 2= moderate levels of stress; note in PyRat, the veterinarian and the project director must be informed, if applicable veterinary care must be initiated	10-19
-Stress level 3= high levels of stress; note in PyRat, with duration the veterinarian and the project director must be informed, veterinary care must be initiated, if applicable the animal must be euthanized or rather the study must be terminated	20 or more

Supplement 2: Detailed Information Concerning the Clinical Sepsis Score

ID	Group	Base	Gav	OP	+0,5	+1	+2	+3	+4	+5	+6	+7	+8
3	Sepsis	0	0	0	12	8	7	7	6	5	4	3	4
5	Control	0	0	0	12	8	4	4	3	1	2	0	0
7	Control	0	0	0	8	4	3	4	4	4	3	1	1
9	Control	0	0	0	6	7	4	3	3	2	1	1	1
11	Sepsis	0	0	0	8	7	8	7	8	7	4	4	4
13	Sepsis	0	0	0	12	8	4	4	2	2	2	3	3
15	Control	0	0	0	11	8	4	4	2	0	0	0	0
17	Sepsis	0	0	0	11	7	7	7	4	2	4	3	3
19	Control	0	0	0	7	8	4	4	2	3	3	3	2
21	Sepsis	0	0	0	7	4	7	8	7	4	3	3	3
23	Sepsis	0	0	0	6	4	4	2	3	4	3	3	3
25	Sepsis	0	0	0	11	8	8	7	6	4	4	2	2
27	Control	0	0	0	8	8	7	4	2	0	1	0	0
29	Sepsis	0	0	0	12	11	8	4	3	2	1	0	1
31	Sepsis	0	0	0	8	8	3	4	4	4	3	3	2
35	Control	0	0	0	12	11	8	7	4	3	2	1	1
37	Control	0	0	0	7	4	3	4	4	4	4	2	2
39	Sepsis	0	0	0	12	8	7	4	2	2	3	2	2

Base…Baseline; Gav…Gavage; OP…Operation